Mathematics

https://www.aimspress.com/journal/Math

AIMS Mathematics, 11(7): 21607–21653.
DOI: 10.3934/math.2026875
Received: 03 May 2026
Revised: 21 June 2026
Accepted: 07 July 2026
Published: 21 July 2026

Research article

A q-rung orthopair spherical fuzzy rough graph approach for modeling uncertain agricultural networks

Wedad Khaled Alshaman and Kholood Mohammad Alsager*

Department of Mathematics, College of Science, Qassim University, Buraydah, Saudi Arabia; 461215344@qu.edu.sa

* **Correspondence:** Email: ksakr@qu.edu.sa.

Abstract: In this paper, we propose a novel hybrid structure termed the q-rung orthopair spherical fuzzy rough graphs (q-ROSFRG) by integrating q-rung orthopair spherical fuzzy sets, rough set theory, and graph theory within rough approximation spaces. The proposed model generalizes classical fuzzy graphs and spherical fuzzy graphs by incorporating q-rung orthopair spherical fuzzy information, which effectively captures positive, neutral, and non-membership degrees under the flexible constraint $[\varsigma]^q + [\varrho]^q + [\varkappa]^q \leq 1$, where $q \geq 1$ is a tunable parameter. We study the basic features of our proposed structure, such as the idempotency of approximation operators, duality by the complement, and connectivity related-inclusions. Furthermore, a group decision-making framework based on the q-ROSFRG model is developed to address uncertain path selection problems in network-based environments. The proposed algorithm handles vagueness and uncertainty in network data through lower and upper approximations combined with a maximin path strength criterion, proceeding iteratively from the source to target nodes. The practicality and efficiency of the suggested method are verified via a real application on agricultural irrigation network selection. In contrast to the existing fuzzy rough models that are designed to pick the best option from a finite set, the q-ROSFRG model tackles a fundamentally different problem: Finding the best connected path in a network while preserving its topological nature.

Keywords: q-rung orthopair fuzzy set; spherical fuzzy set; rough set; fuzzy graph; decision-making
Mathematics Subject Classification: 03B52, 03E72

1. Introduction

Real-world decision-making problems frequently involve various forms of imprecision, vagueness, and incomplete information. Classical mathematical tools often fall short when addressing such complex uncertain environments. To overcome these limitations, several uncertainty modeling frameworks have been developed over the past decades, including fuzzy sets (FS) [1], intuitionistic fuzzy sets (IFS) [2], and rough set (RS) theory [3]. Each of these formalisms, however, exhibits inherent limitations when used independently, which has motivated the development of hybrid approaches that leverage their complementary advantages [4, 5]. The historical evolution of uncertainty modeling can be traced through several key milestones. Zadeh's fuzzy sets [1] introduced the fundamental concept of partial membership degrees. Atanassov's IFS theory [2] extended this paradigm by incorporating both membership and non-membership functions under the constraint $\xi + \zeta \leq 1$, thereby enabling the representation of hesitation. Yager's Pythagorean fuzzy sets (PyFSs) [6] further generalized this framework by relaxing the constraint to a squared sum condition $\xi^2 + \zeta^2 \leq 1$, which expands the space of admissible evaluations. More recently, Mahmood et al. [7] proposed spherical fuzzy sets (SFSs), which introduce a three-dimensional representation incorporating positive, neutral, and negative membership degrees under the constraint $\xi^2 + \varrho^2 + \zeta^2 \leq 1$. As noted by Akram et al. [8], the spherical fuzzy model offers a more versatile framework for capturing complex human judgments and ambiguous real-world phenomena. Subsequently, Yager [9] introduced q-rung orthopair fuzzy sets (q-ROFSs), which generalize PyFSs through a flexible parameter $q \geq 1$ satisfying $\xi^q + \zeta^q \leq 1$. According to Garg [10], increasing the rung parameter q provides greater flexibility in adjusting the admissible region, making q-ROFSs more adaptable than IFSs and picture fuzzy sets (PFSs) for various applications. Building upon these advances, Mahmood et al. developed q-rung orthopair spherical fuzzy sets (q-ROSFSs), which combine the three-dimensional representation of SFSs with the adjustable q-rung constraint $\xi^q + \varrho^q + \zeta^q \leq 1$, offering a powerful and flexible tool for representing positive, neutral, and negative information under tunable uncertainty levels [11]. Concurrently with the advancement of fuzzy set extensions, Molodtsov [12] proposed soft set theory as a generalized mathematical framework for managing uncertainty without the parametric difficulties inherent in traditional approaches. As highlighted by Almozaini and Alsager [13], classical theories face challenges including parameterization complexity, difficulty in handling hybrid uncertainty forms, and limited capacity to address multifaceted real-world problems involving multiple perspectives. Pawlak's RS theory [3] provides a complementary approach for processing granular information and vagueness through the notions of lower and upper approximations. The integration of different uncertainty paradigms has yielded more sophisticated hybrid representations, including rough IFS [14], rough PFSs [15], interval-valued PFSs [16], and interval-valued intuitionistic fuzzy rough sets [17]. As noted by Bilal et al. [18], rough sets inherently exhibit properties as vagueness and indeterminacy from a mathematical perspective.

Graph theory has simultaneously emerged as a powerful tool for modeling complex systems with interacting components. Rosenfeld [19] introduced fuzzy graphs, extending classical graph theory to accommodate vague relations between vertices. Subsequent investigations have explored intuitionistic fuzzy graphs [20], interval-valued fuzzy graphs [21], and spherical fuzzy graphs [8]. Akram and Sitara [22] proposed q-rung orthopair fuzzy graph structures (q-ROFGSs), emphasizing that capturing both positive and negative aspects of information constitutes a vital mechanism for analyzing a system's characteristics within q-rung orthopair fuzzy environments. These graph-based models have found applications across diverse domains, including social network analysis, transportation planning, and communication networks. Azim et al. [23] recently introduced q-spherical fuzzy rough sets (q-SFRs), demonstrating that the integration of q-SFSs with rough sets provides a valuable paradigm for fuzzy mathematics and decision-making. They developed Einstein geometric aggregation operators for image analysis and interpretation. Similarly, Wang et al. [24] investigated the hybrid combination of soft sets and rough sets with q-ROFSs, yielding q-ROF soft rough sets and presenting aggregation operators for multi-criteria decision-making. These developments underscore the growing interest in hybrid frameworks that synergistically combine multiple uncertainty theories.

Recent studies also show that graph-based uncertainty models are moving toward richer network operations and rough-graph approximation mechanisms. Karaaslan and Karamaz [25] developed product operations for T-spherical fuzzy graphs with a multicriteria group decision-making (MCGDM) application, Rao et al. [26] introduced q-rung orthopair fuzzy Zagreb indices for graph-based decision making, and Shi et al. [27] studied fuzzy rough graphs via fuzzy graph ideals. These works are relevant because they combine a fuzzy graph structure with either advanced spherical/q-rung information or rough graph approximations; however, none of them provides a q-rung orthopair spherical fuzzy rough graph (q-ROSFRG) model for source-to-target path selection.

Despite these significant advances, an important research gap remains: The need for an integrated approach that simultaneously addresses multiple dimensions of uncertainty in network-based decision-making by (i) using a flexible q-rung spherical fuzzy structure for modeling fuzziness under adjustable constraints, (ii) incorporating RS approximations to handle granularity and equivalence relations in network data, and (iii) preserving the graph topology and connectivity constraints from source to target nodes. As noted by Azim et al. [23], while traditional fuzzy sets help manage uncertainty, they struggle to capture complex information and effectively represent decision-makers' preferences. Unlike existing hybrid models that focus on selecting the best alternative from a discrete set (e.g., supplier selection, personnel evaluation, or city strategy ranking), real-world applications such as water distribution networks, power grids, transportation systems, and telecommunication routing require identifying the optimal connected path between the source and destination, where the failure of any single edge may compromise the entire route. The present paper addresses this gap by introducing the q-ROSFRG model. Figure 1 illustrates the conceptual integration of these three paradigms.

The main contributions of this paper are as follows. First, we introduce the q-ROSFRG model as a general approach for addressing higher-order vagueness in network-based decision-making under complex uncertain environments, generalizing classical fuzzy graphs by integrating q-rung orthopair SFSs with rough approximations while preserving the flexibility of the q parameter and the granularity handling capabilities of equivalence relations. Second, we establish the fundamental definitions, operations, and theoretical properties of the q-ROSFRG model, including lower and upper approximations for vertices and edges, algebraic operations ($\oplus$, $\otimes$), score and accuracy functions, vertex degree, path strength and connectedness, similarity measures, Cartesian product, and complement properties, with key mathematical results, including the idempotency of the approximation operators, duality via the complement, and connectivity inclusion relationships, proved rigorously. Third, we develop an efficient path selection methodology under the proposed q-ROSFRG framework incorporating a maximin path strength criterion that is particularly suitable for risk-averse infrastructure planning, where the algorithm systematically transforms expert evaluations into q-ROSFS values, computes the lower and upper approximations on the basis of equivalence classes, enumerates candidate paths, and selects the optimal path using score-based ordering. Fourth, we provide an illustrative example of agricultural irrigation network selection to demonstrate the model's applicability and effectiveness, involving 10 agricultural zones and 20 irrigation channels partitioned into equivalence classes according to soil type. The results show that the proposed model successfully identifies the optimal path with a score of 0.65494, outperforming paths containing weak edges. Fifth, we conduct a comprehensive comparative analysis with existing fuzzy rough models, including the interval-valued picture fuzzy soft rough set (IVPFSRS) [13], spherical fuzzy rough graph (SFRG) [8], q-ROFG [22], rough q-ROFS [18], q-SFRN [23], and q-ROF soft rough set [24] models, demonstrating that the q-ROSFRG achieves superior discriminative power, stable ranking performance under input perturbations, and the unique ability to preserve the graph's topology and connectivity constraints.

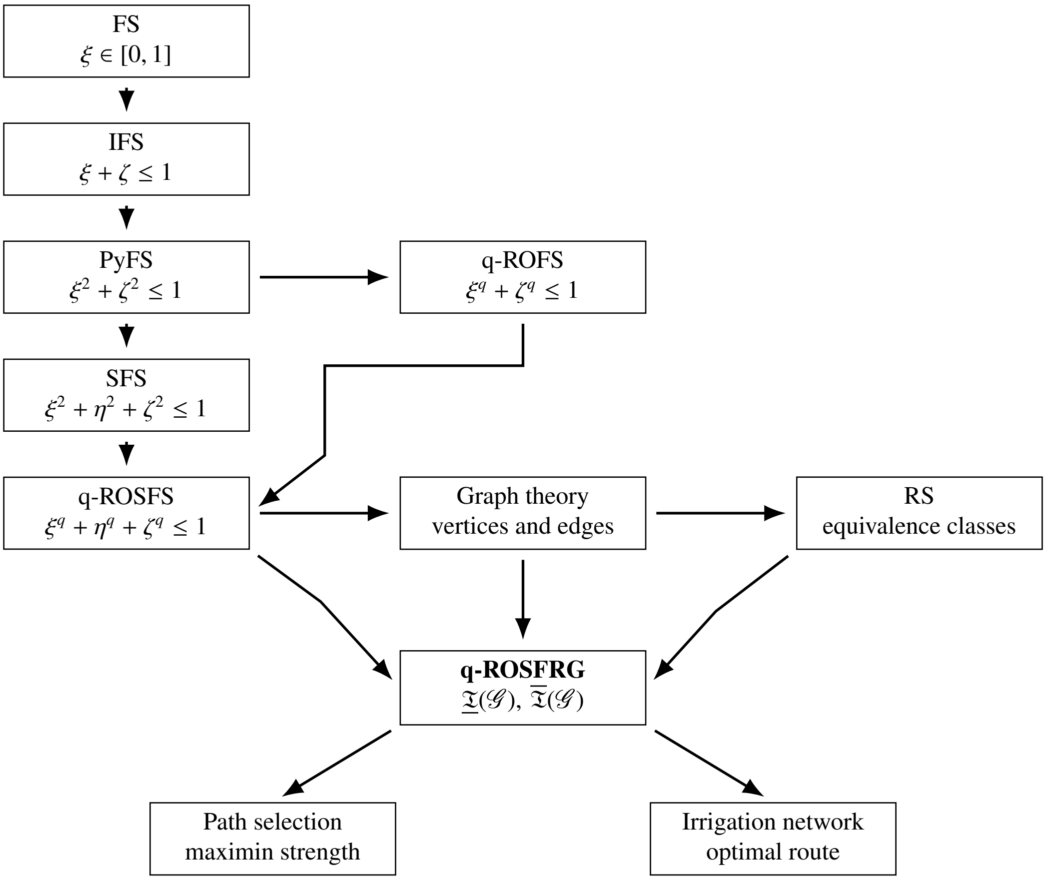

Figure 1. Conceptual workflow of the proposed q-ROSFRG model for uncertainty-aware irrigation path selection.

The remainder of this paper is organized as follows. Section 2 provides the necessary background and preliminaries, including fuzzy sets, IFSs, SFSs, q-ROFSs, q-ROSFSs, fuzzy graphs, and rough sets. Section 3 formally defines the novel concept of the q-ROSFRG; discusses their main operations and types; defines their degree, path, connectedness, similarity measures, and Cartesian product; and proves several algebraic properties, including idempotency and duality. Section 4 presents a comprehensive integrated path selection methodology based on the q-ROSFRG framework with a detailed case study of agricultural irrigation network selection. A qualitative comparative study between the proposed method and other existing approaches is presented in Section 5. Section 6 provides a quantitative comparison and analysis of its performance, computational complexity, and robustness. Finally, Section 7 concludes by summarizing our contributions and their implications, discussing the limitations, and identifying potential avenues for future research. Table 1 presents the main notations used throughout this paper for clarity and reference.

Table 1. List of notations.

Symbol	Description
$\aleph$	Vertex universe (agricultural zones / network nodes)
ℓ	Edge collection (irrigation channels / connections)
$\mathscr{G}^* = (\aleph, \ell)$	Base crisp graph structure
$\mathscr{G} = (\Upsilon, \Delta)$	q-ROSFRG
$\varphi, \omega, \wp$	Individual vertices (nodes in the network)
$\varphi\omega$	Edge linking the vertices φ and ω
$\simeq$	Indiscernibility (equivalence) relation on $\aleph$
$[\varphi]_{\simeq}$	Equivalence class of φ (e.g., by soil type)
$\varsigma_{\Upsilon}(\varphi)$	Positive membership of vertex φ
$\varrho_{\Upsilon}(\varphi)$	Neutral membership of vertex φ
$\varkappa_{\Upsilon}(\varphi)$	Negative membership of vertex φ
$\varsigma_{\Delta}(\varphi\omega)$	Positive membership of edge $\varphi\omega$
$\varrho_{\Delta}(\varphi\omega)$	Neutral membership of edge $\varphi\omega$
$\varkappa_{\Delta}(\varphi\omega)$	Negative membership of edge $\varphi\omega$
$\underline{\mathfrak{B}}_{\varsigma}(\varphi)$	Lower approximation (positive) for vertex φ
$\overline{\mathfrak{B}}_{\varsigma}(\varphi)$	Upper approximation (positive) for vertex φ
$\underline{\mathfrak{B}}_{\varrho}(\varphi)$	Lower approximation (neutral) for vertex φ
$\overline{\mathfrak{B}}_{\varrho}(\varphi)$	Upper approximation (neutral) for vertex φ
$\underline{\mathfrak{B}}_{\varkappa}(\varphi)$	Lower approximation (negative) for vertex φ
$\overline{\mathfrak{B}}_{\varkappa}(\varphi)$	Upper approximation (negative) for vertex φ
$\underline{\mathfrak{E}}_{\varsigma}(\varphi\omega)$	Lower approximation (positive) for edge $\varphi\omega$
$\overline{\mathfrak{E}}_{\varsigma}(\varphi\omega)$	Upper approximation (positive) for edge $\varphi\omega$
$\underline{\mathfrak{E}}_{\varrho}(\varphi\omega)$	Lower approximation (neutral) for edge $\varphi\omega$
$\overline{\mathfrak{E}}_{\varrho}(\varphi\omega)$	Upper approximation (neutral) for edge $\varphi\omega$
$\underline{\mathfrak{E}}_{\varkappa}(\varphi\omega)$	Lower approximation (negative) for edge $\varphi\omega$
$\overline{\mathfrak{E}}_{\varkappa}(\varphi\omega)$	Upper approximation (negative) for edge $\varphi\omega$
q	Rung parameter (integer $q \geq 1$)
$\oplus$	Algebraic sum (addition) operator
$\otimes$	Algebraic product (multiplication) operator
$\cup$	Set-theoretic union
$\cap$	Set-theoretic intersection
$\sim$	Complement operator
$\mathcal{S}(\cdot)$	Score evaluation function
$\mathcal{H}(\cdot)$	Accuracy evaluation function
$\delta(\varphi)$	Degree measure of vertex φ
$\Psi(\varpi)$	Path strength (minimum membership along the path)
σ, ϵ	Origin and destination vertices
q-ROSFRG	q-rung orthopair spherical fuzzy rough graph
q-ROSFS	q-rung orthopair spherical fuzzy sets
MCGDM	Multicriteria group decision-making

2. Preliminaries

This section recalls the essential definitions of fuzzy sets, IFSs, SFSs, q-ROFSs, q-ROSFSs, fuzzy graphs, and RSs, which form the foundational building blocks for the proposed q-ROSFRG model.

Definition 1. *[1] Let $\mathfrak{X}$ be a non-empty universal set. A fuzzy set Θ on $\mathfrak{X}$ is defined as*

$$\Theta = \{\langle \varphi,\ \xi_\Theta(\varphi)\rangle \mid \varphi \in \mathfrak{X}\},$$

where the mapping ξ_Θ: $\mathfrak{X} \to [0,1]$ is referred to as the membership function.

Definition 2. *[2] Let $\mathfrak{X}$ be a non-empty universal set. An IFS Θ on $\mathfrak{X}$ takes the form*

$$\Theta = \{\langle \varphi,\ \xi_\Theta(\varphi),\ \zeta_\Theta(\varphi)\rangle \mid \varphi \in \mathfrak{X}\},$$

where ξ_Θ, ζ_Θ: $\mathfrak{X} \to [0,1]$ satisfy the admissibility condition

$$0 \leq \xi_\Theta(\varphi) + \zeta_\Theta(\varphi) \leq 1, \quad \forall \varphi \in \mathfrak{X}.$$

The degree of hesitation (or indeterminacy) is then given by

$$\Omega_\Theta(\varphi) = 1 - \xi_\Theta(\varphi) - \zeta_\Theta(\varphi).$$

This formulation captures uncertainty by explicitly accommodating a hesitation margin alongside the membership and non-membership evaluations.

Definition 3. *[7] Let $\mathfrak{X}$ be a non-empty universal set. A SFS Θ on $\mathfrak{X}$ is expressed as*

$$\Theta = \{\langle \varphi,\ \varsigma_\Theta(\varphi),\ \varrho_\Theta(\varphi),\ \varkappa_\Theta(\varphi)\rangle \mid \varphi \in \mathfrak{X}\},$$

where $\varsigma_\Theta, \varrho_\Theta, \varkappa_\Theta$: $\mathfrak{X} \to [0,1]$ satisfy the spherical constraint

$$0 \leq \varsigma_\Theta(\varphi)^2 + \varrho_\Theta(\varphi)^2 + \varkappa_\Theta(\varphi)^2 \leq 1, \quad \forall \varphi \in \mathfrak{X}.$$

The refusal (indeterminacy) degree is computed as

$$\pi_\Theta(\varphi) = \sqrt{1 - (\varsigma_\Theta(\varphi)^2 + \varrho_\Theta(\varphi)^2 + \varkappa_\Theta(\varphi)^2)}.$$

Here, the refusal degree is denoted by π to avoid any conflict with the negative membership symbol $\varkappa$. This model enables the simultaneous representation of positive (acceptance), neutral, and negative (rejection) information, thereby offering a more nuanced description of uncertainty compared with earlier frameworks.

Example 1. *Let $\mathfrak{X} = \{\varphi_1, \varphi_2, \varphi_3, \varphi_4\}$. Consider the spherical fuzzy set Θ defined by*

$$\Theta = \{\langle \varphi_1, 0.8, 0.1, 0.1\rangle,\ \langle \varphi_2, 0.7, 0.2, 0.1\rangle, \langle \varphi_3, 0.5, 0.3, 0.2\rangle,\ \langle \varphi_4, 0.6, 0.2, 0.1\rangle\}.$$

We verify the spherical constraint for each element

$$\begin{aligned}\varphi_1 &: 0.8^2 + 0.1^2 + 0.1^2 = 0.64 + 0.01 + 0.01 = 0.66 \leq 1,\\ \varphi_2 &: 0.7^2 + 0.2^2 + 0.1^2 = 0.49 + 0.04 + 0.01 = 0.54 \leq 1,\\ \varphi_3 &: 0.5^2 + 0.3^2 + 0.2^2 = 0.25 + 0.09 + 0.04 = 0.38 \leq 1,\\ \varphi_4 &: 0.6^2 + 0.2^2 + 0.1^2 = 0.36 + 0.04 + 0.01 = 0.41 \leq 1.\end{aligned}$$

The corresponding refusal degrees are

$$\begin{aligned}\pi(\varphi_1) &= \sqrt{1 - 0.66} \approx 0.583,\\ \pi(\varphi_2) &= \sqrt{1 - 0.54} \approx 0.678,\\ \pi(\varphi_3) &= \sqrt{1 - 0.38} \approx 0.787,\\ \pi(\varphi_4) &= \sqrt{1 - 0.41} \approx 0.768.\end{aligned}$$

Thus, each element receives a triple of positive, neutral, and negative membership degrees, demonstrating how SFSs capture more refined uncertainty patterns than traditional fuzzy models.

Definition 4. *[9] Let $\mathfrak{X}$ be a nonempty universal set and let $q \geq 1$ be a fixed real parameter. A q-ROFS Θ on $\mathfrak{X}$ is defined as*

$$\Theta = \{\langle \varphi, \xi_\Theta(\varphi), \zeta_\Theta(\varphi) \rangle \mid \varphi \in \mathfrak{X}\},$$

where ξ_Θ, ζ_Θ: $\mathfrak{X} \to [0, 1]$ satisfy the generalized orthopair condition

$$0 \leq [\xi_\Theta(\varphi)]^q + [\zeta_\Theta(\varphi)]^q \leq 1, \quad \forall \varphi \in \mathfrak{X}.$$

The hesitation degree is derived as follows:

$$\Omega_\Theta(\varphi) = \sqrt[q]{1 - ([\xi_\Theta(\varphi)]^q + [\zeta_\Theta(\varphi)]^q)}.$$

When $q = 1$, the q-ROFS reduces precisely to the IFS. This generalization replaces the linear constraint $\xi + \zeta \leq 1$ with the parametric condition $\xi^q + \zeta^q \leq 1$, thereby providing greater flexibility in representing uncertainty across different application contexts.

Example 2. *Let $\mathfrak{X} = \{\varphi_1, \varphi_2, \varphi_3\}$ represent a collection of agricultural zones, and set $q = 3$. Consider the q-ROFS defined on $\mathfrak{X}$ as follows:*

$$\Theta = \{\langle \varphi_1, 0.9, 0.3 \rangle, \langle \varphi_2, 0.7, 0.6 \rangle, \langle \varphi_3, 0.5, 0.8 \rangle\}.$$

We verify the q-rung constraint for each element:

$$\begin{aligned}\varphi_1 &: 0.9^3 + 0.3^3 = 0.729 + 0.027 = 0.756 \leq 1,\\ \varphi_2 &: 0.7^3 + 0.6^3 = 0.343 + 0.216 = 0.559 \leq 1,\\ \varphi_3 &: 0.5^3 + 0.8^3 = 0.125 + 0.512 = 0.637 \leq 1.\end{aligned}$$

All elements satisfy the q-rung orthopair condition, confirming that Θ constitutes a valid q-ROFS. This example illustrates how increasing the parameter q permits larger independent values for membership and non-membership, thereby expanding the expressiveness of the uncertainty representation.

Definition 5. *[11] Let $q \geq 1$ be a fixed real number and let $\mathfrak{X} \neq \emptyset$ be a universal set. A q-ROSFS Θ on $\mathfrak{X}$ is defined as follows:*

$$\Theta = \{\langle \varphi, \varsigma_\Theta(\varphi), \varrho_\Theta(\varphi), \varkappa_\Theta(\varphi)\rangle \mid \varphi \in \mathfrak{X}\},$$

where $\varsigma_\Theta, \varrho_\Theta, \varkappa_\Theta$: $\mathfrak{X} \to [0,1]$ denote the positive membership, neutral membership, and negative membership functions, respectively, satisfying the q-rung spherical admissibility condition:

$$[\varsigma_\Theta(\varphi)]^q + [\varrho_\Theta(\varphi)]^q + [\varkappa_\Theta(\varphi)]^q \leq 1, \quad \forall \varphi \in \mathfrak{X}.$$

The refusal (indeterminacy) degree is defined as follows:

$$\pi_\Theta(\varphi) = \sqrt[q]{1 - ([\varsigma_\Theta(\varphi)]^q + [\varrho_\Theta(\varphi)]^q + [\varkappa_\Theta(\varphi)]^q)}.$$

Again, π denotes only the refusal degree, while $\varkappa$ denotes negative membership. This concept generalizes the SFS (recovered when $q = 2$) and reduces to a q-ROFS when $\varrho_\Theta(\varphi) = 0$ for all $\varphi \in \mathfrak{X}$. The framework thus extends the SFS through a q-rung structure, offering enhanced flexibility in describing positive, neutral, and negative information under uncertainty.

Example 3. *Let $\mathfrak{X} = \{\varphi_1, \varphi_2, \varphi_3\}$ represent a set of agricultural zones, and take $q = 3$. Consider the q-ROSFS*

$$\Theta = \{\langle \varphi_1, 0.8, 0.2, 0.1\rangle, \langle \varphi_2, 0.7, 0.3, 0.2\rangle, \langle \varphi_3, 0.6, 0.2, 0.3\rangle\}.$$

Verification of the q-rung spherical condition yields:

$$\begin{aligned}
\varphi_1 &: 0.8^3 + 0.2^3 + 0.1^3 = 0.512 + 0.008 + 0.001 = 0.521 \leq 1, \\
\varphi_2 &: 0.7^3 + 0.3^3 + 0.2^3 = 0.343 + 0.027 + 0.008 = 0.378 \leq 1, \\
\varphi_3 &: 0.6^3 + 0.2^3 + 0.3^3 = 0.216 + 0.008 + 0.027 = 0.251 \leq 1.
\end{aligned}$$

All elements satisfy the q-rung spherical constraint, confirming that Θ is a valid q-ROSFS. This example demonstrates how each agricultural entity can simultaneously hold positive, neutral, and negative information under uncertainty, providing a more realistic representation than classical fuzzy models.

Definition 6. *[19] Let $\aleph$ be a non-empty vertex set. A fuzzy graph $\mathscr{G} = (\Upsilon, \Delta)$ consists of a fuzzy set Υ defined on $\aleph$ and a fuzzy set Δ defined on $\aleph \times \aleph$ such that for all $\omega, \wp \in \aleph$, we have*

$$\xi_\Delta(\omega\wp) \leq \min\left(\xi_\Upsilon(\omega), \xi_\Upsilon(\wp)\right).$$

Definition 7. *Let $\aleph$ be a nonempty vertex set. A q-rung orthopair spherical fuzzy graph (q-ROSFG) on $\aleph$ is a pair $\mathscr{G} = (\Upsilon, \Delta)$ where*

- $\Upsilon = \{\langle \varphi, \varsigma_\Upsilon(\varphi), \varrho_\Upsilon(\varphi), \varkappa_\Upsilon(\varphi)\rangle \mid \varphi \in \aleph\}$ *is a q-ROSFS on the vertex set,*
- $\Delta = \{\langle \omega\wp, \varsigma_\Delta(\omega\wp), \varrho_\Delta(\omega\wp), \varkappa_\Delta(\omega\wp)\rangle \mid \omega, \wp \in \aleph\}$ *is a q-ROSFS on the edge set,*

subject to the following consistency conditions for all $\omega, \wp \in \aleph$:

$$\begin{aligned}
\varsigma_\Delta(\omega\wp) &\leq \min\left(\varsigma_\Upsilon(\omega), \varsigma_\Upsilon(\wp)\right), \\
\varrho_\Delta(\omega\wp) &\leq \min\left(\varrho_\Upsilon(\omega), \varrho_\Upsilon(\wp)\right), \\
\varkappa_\Delta(\omega\wp) &\geq \max\left(\varkappa_\Upsilon(\omega), \varkappa_\Upsilon(\wp)\right),
\end{aligned}$$

and the following q-rung spherical condition must hold:

$$\varsigma_\Delta(\omega\wp)^q + \varrho_\Delta(\omega\wp)^q + \varkappa_\Delta(\omega\wp)^q \leq 1.$$

This structure models networks where both the vertices and edges carry positive, neutral, and negative information under uncertainty, enabling a richer and more realistic representation of complex systems such as agricultural irrigation networks.

Remark 1. *The condition* $\varkappa_\Delta(\omega\wp) \geq \max(\varkappa_\Upsilon(\omega), \varkappa_\Upsilon(\wp))$ *reflects realistic scenarios in applications like agricultural networks. The negative membership (e.g., the risk, cost, or environmental impact) of an irrigation channel is typically at least as severe as that of its incident zones, since connecting two zones may exacerbate harmful aspects.*

Example 4. *Let* $\aleph = \{\varphi_1, \varphi_2, \varphi_3\}$ *and* $q = 2$. *Consider the q-ROSFG* $\mathscr{G} = (\Upsilon, \Delta)$ *defined by*

$$\begin{aligned} \Upsilon(\varphi_1) &= \langle 0.8, 0.1, 0.1\rangle, & \Delta(\varphi_1\varphi_2) &= \langle 0.7, 0.1, 0.1\rangle, \\ \Upsilon(\varphi_2) &= \langle 0.7, 0.2, 0.1\rangle, & \Delta(\varphi_2\varphi_3) &= \langle 0.6, 0.2, 0.2\rangle, \\ \Upsilon(\varphi_3) &= \langle 0.6, 0.2, 0.2\rangle, & \Delta(\varphi_1\varphi_3) &= \langle 0.6, 0.1, 0.2\rangle. \end{aligned}$$

Figure 2 illustrates the corresponding q-ROSFG.

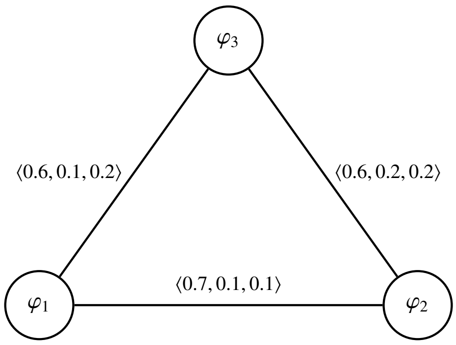

Figure 2. A q-ROSFG with $q = 2$.

Verification of the q-rung spherical condition for each edge is as follows:

$$\begin{aligned} 0.7^2 + 0.1^2 + 0.1^2 &= 0.49 + 0.01 + 0.01 = 0.51 \leq 1, \\ 0.6^2 + 0.2^2 + 0.2^2 &= 0.36 + 0.04 + 0.04 = 0.44 \leq 1, \\ 0.6^2 + 0.1^2 + 0.2^2 &= 0.36 + 0.01 + 0.04 = 0.41 \leq 1. \end{aligned}$$

Thus, $\mathscr{G}$ *is a valid q-ROSFG. This example illustrates how a network can be modeled using q-rung orthopair spherical fuzzy information, where each vertex and edge is characterized by positive, neutral, and negative membership values under uncertainty.*

Definition 8. *[3] Let* $\mathfrak{X}$ *be a non-empty universal set equipped with an equivalence relation* $\simeq$. *The pair* $(\mathfrak{X}, \simeq)$ *constitutes a Pawlak approximation space. For any* $\varphi \in \mathfrak{X}$, *the equivalence class containing*

φ is denoted $[\varphi]_{\simeq} = \{\omega \in \mathfrak{X} \mid (\varphi, \omega) \in \simeq\}$. For any subset $\mathfrak{Z} \subseteq \mathfrak{X}$, the lower and upper approximations are defined, respectively, as follows:

$$\underline{\mathfrak{T}}(\mathfrak{Z}) = \{\varphi \in \mathfrak{X} \mid [\varphi]_{\simeq} \subseteq \mathfrak{Z}\}, \qquad \overline{\mathfrak{T}}(\mathfrak{Z}) = \{\varphi \in \mathfrak{X} \mid [\varphi]_{\simeq} \cap \mathfrak{Z} \neq \emptyset\}.$$

If $\underline{\mathfrak{T}}(\mathfrak{Z}) = \overline{\mathfrak{T}}(\mathfrak{Z})$, then $\mathfrak{Z}$ is called definable; otherwise, the pair $(\underline{\mathfrak{T}}(\mathfrak{Z}), \overline{\mathfrak{T}}(\mathfrak{Z}))$ forms an RS.

Definition 9. *[28] Let $\mathscr{G}^* = (\aleph, \ell)$ be a crisp graph and let $\simeq$ be an equivalence relation defined on $\aleph$. For any subgraph $\imath \subseteq \mathscr{G}^*$, the lower approximation $\underline{\mathfrak{T}}(\imath)$ and upper approximation $\overline{\mathfrak{T}}(\imath)$ are given by:*

$$\underline{\mathfrak{T}}(\imath) = (\underline{\mathfrak{T}}(\aleph_\imath), \underline{\mathfrak{T}}(\ell_\imath)), \quad \overline{\mathfrak{T}}(\imath) = (\overline{\mathfrak{T}}(\aleph_\imath), \overline{\mathfrak{T}}(\ell_\imath)),$$

where

$$\underline{\mathfrak{T}}(\aleph_\imath) = \{\varphi \in \aleph \mid [\varphi]_{\simeq} \subseteq \aleph_\imath\},$$
$$\overline{\mathfrak{T}}(\aleph_\imath) = \{\varphi \in \aleph \mid [\varphi]_{\simeq} \cap \aleph_\imath \neq \emptyset\},$$

and for the edges $\omega\wp \in \underline{\mathfrak{T}}(\ell_\imath)$ if and only if $[\omega]_{\simeq} \times [\wp]_{\simeq} \subseteq \ell_\imath$, while $\omega\wp \in \overline{\mathfrak{T}}(\ell_\imath)$ if and only if $([\omega]_{\simeq} \times [\wp]_{\simeq}) \cap \ell_\imath \neq \emptyset$. If $\underline{\mathfrak{T}}(\imath) = \overline{\mathfrak{T}}(\imath)$, then $\imath$ is termed definable; otherwise, the pair $(\underline{\mathfrak{T}}(\imath), \overline{\mathfrak{T}}(\imath))$ is called a rough graph.

3. The q-ROSFRG model

This section introduces the q-ROSFRG model. The model starts from a q-ROSFG), then applies rough lower and upper approximations induced by an equivalence relation on the vertex universe. In this way, the q-ROSFRG preserves the graph topology while distinguishing certain information, represented by the lower approximation, from possible information, represented by the upper approximation.

The derivation is as follows. First, a crisp graph $\mathscr{G}^* = (\aleph, \ell)$ fixes the admissible adjacency pattern. Second, each vertex and each admissible edge is assigned a q-ROSFS value $\langle \varsigma, \varrho, \varkappa \rangle$, producing a q-ROSFG $\mathscr{G} = (\Upsilon, \Delta)$. Third, an equivalence relation $\simeq$ partitions the vertices into granules $[\varphi]_{\simeq}$; for example, zones with similar soil characteristics. Finally, the q-ROSFG is transformed into the pair $(\underline{\mathfrak{T}}(\mathscr{G}), \overline{\mathfrak{T}}(\mathscr{G}))$ by aggregating the q-ROSFS values within these granules. This construction explains how the q-ROSFRG is derived from q-ROSFG rather than being introduced as an independent structure.

Definition 10. *Let $\mathscr{G}^* = (\aleph, \ell)$ be a crisp graph and suppose $\simeq$ is an equivalence relation defined on $\aleph$. Consider a q-ROSFG $\mathscr{G} = (\Upsilon, \Delta)$ constructed over $\mathscr{G}^*$. For each equivalence class $[\varphi]_{\simeq} = \{\omega \in \aleph \mid \omega \simeq \varphi\}$, we construct two derived structures:*

- *The lower approximation $\underline{\mathfrak{T}}(\mathscr{G}) = (\underline{\mathfrak{V}}, \underline{\mathfrak{E}})$ captures information that is certain across the class.*
- *The upper approximation $\overline{\mathfrak{T}}(\mathscr{G}) = (\overline{\mathfrak{V}}, \overline{\mathfrak{E}})$ captures information that is possible within the class.*

(1) Vertex approximations: for any vertex $\varphi \in \aleph$

$$\begin{aligned}
&\underline{\mathfrak{V}}_{\varsigma}(\varphi) = \bigwedge_{\omega\in[\varphi]_{\simeq}} \varsigma_{\Upsilon}(\omega), \qquad \overline{\mathfrak{V}}_{\varsigma}(\varphi) = \bigvee_{\omega\in[\varphi]_{\simeq}} \varsigma_{\Upsilon}(\omega),\\
&\underline{\mathfrak{V}}_{\varrho}(\varphi) = \bigwedge_{\omega\in[\varphi]_{\simeq}} \varrho_{\Upsilon}(\omega), \qquad \overline{\mathfrak{V}}_{\varrho}(\varphi) = \bigvee_{\omega\in[\varphi]_{\simeq}} \varrho_{\Upsilon}(\omega),\\
&\underline{\mathfrak{V}}_{\varkappa}(\varphi) = \bigvee_{\omega\in[\varphi]_{\simeq}} \varkappa_{\Upsilon}(\omega), \qquad \overline{\mathfrak{V}}_{\varkappa}(\varphi) = \bigwedge_{\omega\in[\varphi]_{\simeq}} \varkappa_{\Upsilon}(\omega).
\end{aligned} \tag{3.1}$$

(2) Edge approximations: for any edge $\omega\wp \in \ell$

$$\begin{aligned}
&\underline{\mathfrak{E}}_{\varsigma}(\omega\wp) = \bigwedge_{\varphi\in[\omega]_{\simeq}} \bigwedge_{\varphi'\in[\wp]_{\simeq}} \varsigma_{\Delta}(\varphi\varphi'), \qquad \overline{\mathfrak{E}}_{\varsigma}(\omega\wp) = \bigvee_{\varphi\in[\omega]_{\simeq}} \bigvee_{\varphi'\in[\wp]_{\simeq}} \varsigma_{\Delta}(\varphi\varphi'),\\
&\underline{\mathfrak{E}}_{\varrho}(\omega\wp) = \bigwedge_{\varphi\in[\omega]_{\simeq}} \bigwedge_{\varphi'\in[\wp]_{\simeq}} \varrho_{\Delta}(\varphi\varphi'), \qquad \overline{\mathfrak{E}}_{\varrho}(\omega\wp) = \bigvee_{\varphi\in[\omega]_{\simeq}} \bigvee_{\varphi'\in[\wp]_{\simeq}} \varrho_{\Delta}(\varphi\varphi'),\\
&\underline{\mathfrak{E}}_{\varkappa}(\omega\wp) = \bigvee_{\varphi\in[\omega]_{\simeq}} \bigvee_{\varphi'\in[\wp]_{\simeq}} \varkappa_{\Delta}(\varphi\varphi'), \qquad \overline{\mathfrak{E}}_{\varkappa}(\omega\wp) = \bigwedge_{\varphi\in[\omega]_{\simeq}} \bigwedge_{\varphi'\in[\wp]_{\simeq}} \varkappa_{\Delta}(\varphi\varphi').
\end{aligned} \tag{3.2}$$

These approximations must satisfy the following q-rung spherical consistency conditions:

$$\begin{aligned}
&0 \le \left[\underline{\mathfrak{V}}_{\varsigma}(\varphi)\right]^q + \left[\underline{\mathfrak{V}}_{\varrho}(\varphi)\right]^q + \left[\underline{\mathfrak{V}}_{\varkappa}(\varphi)\right]^q \le 1,\\
&0 \le \left[\overline{\mathfrak{V}}_{\varsigma}(\varphi)\right]^q + \left[\overline{\mathfrak{V}}_{\varrho}(\varphi)\right]^q + \left[\overline{\mathfrak{V}}_{\varkappa}(\varphi)\right]^q \le 1,\\
&0 \le \left[\underline{\mathfrak{E}}_{\varsigma}(\omega\wp)\right]^q + \left[\underline{\mathfrak{E}}_{\varrho}(\omega\wp)\right]^q + \left[\underline{\mathfrak{E}}_{\varkappa}(\omega\wp)\right]^q \le 1,\\
&0 \le \left[\overline{\mathfrak{E}}_{\varsigma}(\omega\wp)\right]^q + \left[\overline{\mathfrak{E}}_{\varrho}(\omega\wp)\right]^q + \left[\overline{\mathfrak{E}}_{\varkappa}(\omega\wp)\right]^q \le 1.
\end{aligned} \tag{3.3}$$

If $\underline{\mathfrak{T}}(\mathscr{G}) = \overline{\mathfrak{T}}(\mathscr{G})$, then $\mathscr{G}$ is called definable with respect to $\simeq$; otherwise, the pair $(\underline{\mathfrak{T}}(\mathscr{G}), \overline{\mathfrak{T}}(\mathscr{G}))$ constitutes a q-ROSFRG.

Example 5. *Let $\aleph = \{\varphi_1, \varphi_2, \varphi_3, \varphi_4\}$ and let the crisp edge set be*

$$\ell = \{\varphi_1\varphi_3, \varphi_2\varphi_3, \varphi_3\varphi_4\}.$$

Assume that the equivalence relation $\simeq$ partitions the vertices into

$$[\varphi_1]_{\simeq} = [\varphi_2]_{\simeq} = \{\varphi_1, \varphi_2\}, \quad [\varphi_3]_{\simeq} = \{\varphi_3\}, \quad [\varphi_4]_{\simeq} = \{\varphi_4\}.$$

For $q = 2$, define the q-OSFG $\mathscr{G} = (\Upsilon, \Delta)$ as

$$\begin{aligned}
\Upsilon(\varphi_1) = \langle 0.80, 0.10, 0.10\rangle, \quad \Upsilon(\varphi_2) = \langle 0.70, 0.20, 0.10\rangle,\\
\Upsilon(\varphi_3) = \langle 0.50, 0.30, 0.20\rangle, \quad \Upsilon(\varphi_4) = \langle 0.60, 0.20, 0.20\rangle,
\end{aligned}$$

and

$$\begin{aligned}
\Delta(\varphi_1\varphi_3) = \langle 0.55, 0.10, 0.20\rangle,\\
\Delta(\varphi_2\varphi_3) = \langle 0.45, 0.25, 0.30\rangle,\\
\Delta(\varphi_3\varphi_4) = \langle 0.30, 0.30, 0.40\rangle.
\end{aligned}$$

The equivalence class $\{\varphi_1, \varphi_2\}$ *is non-singleton, so it produces a genuinely rough approximation. For instance,*

$$\underline{\mathfrak{B}}_{\varsigma}(\varphi_1) = 0.80 \wedge 0.70 = 0.70, \quad \overline{\mathfrak{B}}_{\varsigma}(\varphi_1) = 0.80 \vee 0.70 = 0.80,$$
$$\underline{\mathfrak{B}}_{\varrho}(\varphi_1) = 0.10 \wedge 0.20 = 0.10, \quad \overline{\mathfrak{B}}_{\varrho}(\varphi_1) = 0.10 \vee 0.20 = 0.20,$$
$$\underline{\mathfrak{B}}_{\varkappa}(\varphi_1) = 0.10 \vee 0.10 = 0.10, \quad \overline{\mathfrak{B}}_{\varkappa}(\varphi_1) = 0.10 \wedge 0.10 = 0.10.$$

Thus, the neutral upper approximation is computed by the maximum operator, $0.10 \vee 0.20 = 0.20$*, not by the minimum operator.*

Figure 3 illustrates the corresponding q-ROSFRG approximation.

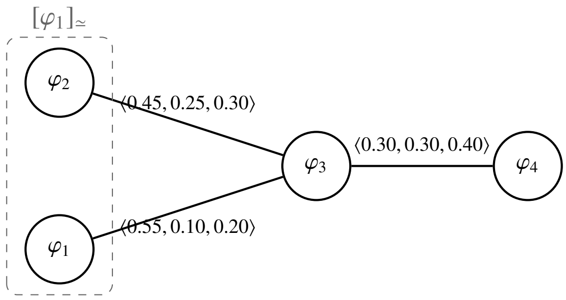

Figure 3. Nontrivial q-ROSFRG approximation generated by a two-vertex equivalence class.

For the edge class between $[\varphi_1]_{\simeq}$ *and* $[\varphi_3]_{\simeq}$*, the two possible representatives are* $\varphi_1\varphi_3$ *and* $\varphi_2\varphi_3$*. Therefore, we have*

$$\underline{\mathfrak{E}}(\varphi_1\varphi_3) = \langle 0.45, 0.10, 0.30\rangle,$$
$$\overline{\mathfrak{E}}(\varphi_1\varphi_3) = \langle 0.55, 0.25, 0.20\rangle.$$

The singleton edge $\varphi_3\varphi_4$ *remains unchanged in both approximations. Table 2 summarizes the nontrivial vertex and edge approximations.*

Table 2. Corrected nontrivial lower and upper approximations in Example 5.

Object	Lower approximation			Upper approximation		
	ς	ϱ	$\varkappa$	ς	ϱ	$\varkappa$
φ_1, φ_2	0.70	0.10	0.10	0.80	0.20	0.10
$\varphi_1\varphi_3, \varphi_2\varphi_3$	0.45	0.10	0.30	0.55	0.25	0.20

Since at least one lower value differs from its corresponding upper value, $(\underline{\mathfrak{T}}(\mathscr{G}), \overline{\mathfrak{T}}(\mathscr{G}))$ *is a genuine q-ROSFRG rather than a definable q-OSFG.*

Graph-neighbor interpretation. For a vertex φ, the graph-neighbor set is $N(\varphi) = \{\omega \in \aleph \mid \varphi\omega \in \ell\}$. In the q-ROSFRG setting, the rough granule $[\varphi]_{\simeq}$ should be read together with the neighbor structure: The lower approximation retains only the q-ROSFS information that is consistently supported by all indistinguishable representatives in the same granule, whereas the upper approximation retains information supported by at least one possible representative. For an edge $\varphi\omega$, the relevant neighborhood is the product granule $[\varphi]_{\simeq} \times [\omega]_{\simeq}$; hence, the lower edge approximation measures the guaranteed relation between the two neighboring classes, while the upper edge approximation measures the possible relation between them. This view is conceptually related to neighbor-based graph constructions in Type-2 soft graphs but differs in that the present model is q-ROSFS-valued and uses rough equivalence classes to preserve source-to-target network connectivity.

Theorem 1. *Consider a q-ROSFRG* $\mathscr{G} = (\Upsilon, \Delta)$ *defined on the approximation space* $(\aleph, \simeq)$*, and let* λ, η *be any two q-ROSFSs on* $\aleph$*. We write* $\lambda \leq \eta$ *when* $\varsigma_\lambda \leq \varsigma_\eta$*,* $\varrho_\lambda \leq \varrho_\eta$*, and* $\varkappa_\lambda \geq \varkappa_\eta$ *componentwise. Then the following statements hold:*

1) $\underline{\mathfrak{T}}(\aleph) = \aleph = \overline{\mathfrak{T}}(\aleph)$;

2) $\underline{\mathfrak{T}}(\emptyset) = \emptyset = \overline{\mathfrak{T}}(\emptyset)$;

3) If $\lambda \leq \eta$*, then* $\underline{\mathfrak{T}}(\lambda) \leq \underline{\mathfrak{T}}(\eta)$;

4) If $\lambda \leq \eta$*, then* $\overline{\mathfrak{T}}(\lambda) \leq \overline{\mathfrak{T}}(\eta)$;

5) $\underline{\mathfrak{T}}(\lambda) =\sim \overline{\mathfrak{T}}(\sim \lambda)$;

6) $\overline{\mathfrak{T}}(\lambda) =\sim \underline{\mathfrak{T}}(\sim \lambda)$;

7) $\underline{\mathfrak{T}}(\lambda \wedge \eta) = \underline{\mathfrak{T}}(\lambda) \wedge \underline{\mathfrak{T}}(\eta)$;

8) $\overline{\mathfrak{T}}(\lambda \vee \eta) = \overline{\mathfrak{T}}(\lambda) \vee \overline{\mathfrak{T}}(\eta)$;

where $\sim \lambda$ *denotes the complement of* λ*.*

Proof. Statements 1) and 2), namely $\underline{\mathfrak{T}}(\aleph) = \aleph = \overline{\mathfrak{T}}(\aleph)$ and $\underline{\mathfrak{T}}(\emptyset) = \emptyset = \overline{\mathfrak{T}}(\emptyset)$, follow directly from the definitions of the lower and upper approximations. The proofs of statements 3)–5) are given below; the remaining statements can be established similarly.

(3) $(\lambda \leq \eta) \Rightarrow (\underline{\mathfrak{T}}(\lambda) \leq \underline{\mathfrak{T}}(\eta))$

Fix an arbitrary vertex $\varphi \in \aleph$. From $\lambda \leq \eta$, we obtain

$$\varsigma_\lambda(\varphi) \leq \varsigma_\eta(\varphi), \quad \varrho_\lambda(\varphi) \leq \varrho_\eta(\varphi), \quad \varkappa_\lambda(\varphi) \geq \varkappa_\eta(\varphi).$$

Then for any $\varphi \in \aleph$, we have

$$\begin{aligned}
\varsigma_{\underline{\mathfrak{T}}(\lambda)}(\varphi) &= \bigwedge_{\omega \in [\varphi]_\simeq} \varsigma_\lambda(\omega) \leq \bigwedge_{\omega \in [\varphi]_\simeq} \varsigma_\eta(\omega) = \varsigma_{\underline{\mathfrak{T}}(\eta)}(\varphi), \\
\varrho_{\underline{\mathfrak{T}}(\lambda)}(\varphi) &= \bigwedge_{\omega \in [\varphi]_\simeq} \varrho_\lambda(\omega) \leq \bigwedge_{\omega \in [\varphi]_\simeq} \varrho_\eta(\omega) = \varrho_{\underline{\mathfrak{T}}(\eta)}(\varphi), \\
\varkappa_{\underline{\mathfrak{T}}(\lambda)}(\varphi) &= \bigvee_{\omega \in [\varphi]_\simeq} \varkappa_\lambda(\omega) \geq \bigvee_{\omega \in [\varphi]_\simeq} \varkappa_\eta(\omega) = \varkappa_{\underline{\mathfrak{T}}(\eta)}(\varphi).
\end{aligned}$$

Thus $\underline{\mathfrak{T}}(\lambda)(\varphi) \leq \underline{\mathfrak{T}}(\eta)(\varphi)$ holds for all φ, yielding $\underline{\mathfrak{T}}(\lambda) \leq \underline{\mathfrak{T}}(\eta)$.

(4) $(\lambda \subseteq \eta) \Rightarrow (\overline{\mathfrak{T}}(\lambda) \subseteq \overline{\mathfrak{T}}(\eta))$

Using the same assumption $\lambda \subseteq \eta$, for each $\varphi \in \aleph$, we have

$$\varsigma_{\overline{\mathfrak{T}}(\lambda)}(\varphi) = \bigvee_{\omega\in[\varphi]_{\simeq}} \varsigma_{\lambda}(\omega) \leq \bigvee_{\omega\in[\varphi]_{\simeq}} \varsigma_{\eta}(\omega) = \varsigma_{\overline{\mathfrak{T}}(\eta)}(\varphi),$$
$$\varrho_{\overline{\mathfrak{T}}(\lambda)}(\varphi) = \bigvee_{\omega\in[\varphi]_{\simeq}} \varrho_{\lambda}(\omega) \leq \bigvee_{\omega\in[\varphi]_{\simeq}} \varrho_{\eta}(\omega) = \varrho_{\overline{\mathfrak{T}}(\eta)}(\varphi),$$
$$\varkappa_{\overline{\mathfrak{T}}(\lambda)}(\varphi) = \bigwedge_{\omega\in[\varphi]_{\simeq}} \varkappa_{\lambda}(\omega) \geq \bigwedge_{\omega\in[\varphi]_{\simeq}} \varkappa_{\eta}(\omega) = \varkappa_{\overline{\mathfrak{T}}(\eta)}(\varphi).$$

Hence, $\overline{\mathfrak{T}}(\lambda)(\varphi) \leq \overline{\mathfrak{T}}(\eta)(\varphi)$ for all φ, i.e., $\overline{\mathfrak{T}}(\lambda) \subseteq \overline{\mathfrak{T}}(\eta)$.

(5) $\underline{\mathfrak{T}}(\lambda) =\sim \overline{\mathfrak{T}}(\sim \lambda)$

We first compute $\overline{\mathfrak{T}}(\sim \lambda)$. For any $\varphi \in \aleph$, we have

$$\overline{\mathfrak{T}}(\sim \lambda) = \left\{\left\langle \varphi,\ [\varsigma^{L}_{\overline{\mathfrak{T}}(\sim\lambda)}(\varphi), \varsigma^{U}_{\overline{\mathfrak{T}}(\sim\lambda)}(\varphi)], [\varrho^{L}_{\overline{\mathfrak{T}}(\sim\lambda)}(\varphi), \varrho^{U}_{\overline{\mathfrak{T}}(\sim\lambda)}(\varphi)], [\varkappa^{L}_{\overline{\mathfrak{T}}(\sim\lambda)}(\varphi), \varkappa^{U}_{\overline{\mathfrak{T}}(\sim\lambda)}(\varphi)]\right\rangle \mid \varphi \in \aleph\right\}.$$

Applying the complement $\sim$ gives:

$$\sim \overline{\mathfrak{T}}(\sim \lambda) = \left\{\left\langle \varphi,\ [\varkappa^{L}_{\overline{\mathfrak{T}}(\sim\lambda)}(\varphi), \varkappa^{U}_{\overline{\mathfrak{T}}(\sim\lambda)}(\varphi)], [\varrho^{L}_{\overline{\mathfrak{T}}(\sim\lambda)}(\varphi), \varrho^{U}_{\overline{\mathfrak{T}}(\sim\lambda)}(\varphi)], [\varsigma^{L}_{\overline{\mathfrak{T}}(\sim\lambda)}(\varphi), \varsigma^{U}_{\overline{\mathfrak{T}}(\sim\lambda)}(\varphi)]\right\rangle \mid \varphi \in \aleph\right\}.$$

From the definition of the upper approximation for $\sim \lambda$, we have

$$\varsigma^{L}_{\overline{\mathfrak{T}}(\sim\lambda)}(\varphi) = \bigvee_{u\in[\varphi]_{\simeq}} \varsigma^{L}_{\sim\lambda}(u) = \bigvee_{u\in[\varphi]_{\simeq}} \varkappa^{L}_{\lambda}(u),$$
$$\varsigma^{U}_{\overline{\mathfrak{T}}(\sim\lambda)}(\varphi) = \bigvee_{u\in[\varphi]_{\simeq}} \varsigma^{U}_{\sim\lambda}(u) = \bigvee_{u\in[\varphi]_{\simeq}} \varkappa^{U}_{\lambda}(u),$$
$$\varrho^{L}_{\overline{\mathfrak{T}}(\sim\lambda)}(\varphi) = \bigvee_{u\in[\varphi]_{\simeq}} \varrho^{L}_{\sim\lambda}(u) = \bigvee_{u\in[\varphi]_{\simeq}} \varrho^{L}_{\lambda}(u),$$
$$\varrho^{U}_{\overline{\mathfrak{T}}(\sim\lambda)}(\varphi) = \bigvee_{u\in[\varphi]_{\simeq}} \varrho^{U}_{\sim\lambda}(u) = \bigvee_{u\in[\varphi]_{\simeq}} \varrho^{U}_{\lambda}(u),$$
$$\varkappa^{L}_{\overline{\mathfrak{T}}(\sim\lambda)}(\varphi) = \bigwedge_{u\in[\varphi]_{\simeq}} \varkappa^{L}_{\sim\lambda}(u) = \bigwedge_{u\in[\varphi]_{\simeq}} \varsigma^{L}_{\lambda}(u),$$
$$\varkappa^{U}_{\overline{\mathfrak{T}}(\sim\lambda)}(\varphi) = \bigwedge_{u\in[\varphi]_{\simeq}} \varkappa^{U}_{\sim\lambda}(u) = \bigwedge_{u\in[\varphi]_{\simeq}} \varsigma^{U}_{\lambda}(u).$$

Substituting back, we have

$$\sim \overline{\mathfrak{T}}(\sim \lambda) = \left\{\left\langle \varphi, \Big[\bigwedge_{u\in[\varphi]_{\simeq}} \varsigma^{L}_{\lambda}(u), \bigwedge_{u\in[\varphi]_{\simeq}} \varsigma^{U}_{\lambda}(u)\Big], \Big[\bigvee_{u\in[\varphi]_{\simeq}} \varrho^{L}_{\lambda}(u), \bigvee_{u\in[\varphi]_{\simeq}} \varrho^{U}_{\lambda}(u)\Big], \Big[\bigvee_{u\in[\varphi]_{\simeq}} \varkappa^{L}_{\lambda}(u), \bigvee_{u\in[\varphi]_{\simeq}} \varkappa^{U}_{\lambda}(u)\Big]\right\rangle \mid \varphi \in \aleph\right\}.$$

This coincides exactly with the definition of $\underline{\mathfrak{T}}(\lambda)$. Therefore $\underline{\mathfrak{T}}(\lambda) =\sim \overline{\mathfrak{T}}(\sim \lambda)$.

The remaining results follow similarly from the definitions. □

Definition 11. *Let $\mathscr{G} = (\Upsilon, \Delta)$ be a q-ROSFRG defined over the underlying crisp graph $\mathscr{G}^* = (\aleph, \ell)$. We introduce the following classifications based on how edge membership values relate to vertex memberships.*

(1) Strong q-ROSFRG: For every edge $\omega\wp \in \ell$, the following identities are required:

$$\begin{cases} \varsigma_\Delta(\omega\wp) = \min\left(\varsigma_\Upsilon(\omega), \varsigma_\Upsilon(\wp)\right), \\ \varrho_\Delta(\omega\wp) = \min\left(\varrho_\Upsilon(\omega), \varrho_\Upsilon(\wp)\right), \\ \varkappa_\Delta(\omega\wp) = \max\left(\varkappa_\Upsilon(\omega), \varkappa_\Upsilon(\wp)\right). \end{cases}$$

(2) Positive membership-strong q-ROSFRG: For each edge $\omega\wp \in \ell$, we impose:

$$\begin{cases} \varsigma_\Delta(\omega\wp) = \min\left(\varsigma_\Upsilon(\omega), \varsigma_\Upsilon(\wp)\right), \\ \varrho_\Delta(\omega\wp) \leq \min\left(\varrho_\Upsilon(\omega), \varrho_\Upsilon(\wp)\right), \\ \varkappa_\Delta(\omega\wp) \leq \max\left(\varkappa_\Upsilon(\omega), \varkappa_\Upsilon(\wp)\right). \end{cases}$$

(3) Negative membership-strong q-ROSFRG: For every edge $\omega\wp \in \ell$, the conditions become:

$$\begin{cases} \varsigma_\Delta(\omega\wp) \leq \min\left(\varsigma_\Upsilon(\omega), \varsigma_\Upsilon(\wp)\right), \\ \varrho_\Delta(\omega\wp) \leq \min\left(\varrho_\Upsilon(\omega), \varrho_\Upsilon(\wp)\right), \\ \varkappa_\Delta(\omega\wp) = \max\left(\varkappa_\Upsilon(\omega), \varkappa_\Upsilon(\wp)\right). \end{cases}$$

(4) Complete q-ROSFRG: For any two distinct vertices $\omega, \wp \in \aleph$ that are adjacent in $\mathscr{G}^*$ (i.e., $\omega\wp \in \ell$), the equalities from the strong case must hold. Moreover, for any non-adjacent distinct pair $\omega, \wp \notin \ell$, we require:

$$\varsigma_\Delta(\omega\wp) = 0, \quad \varrho_\Delta(\omega\wp) = 0, \quad \varkappa_\Delta(\omega\wp) = 1.$$

These hierarchical definitions characterize the extent to which edge information is determined by vertex values, where stricter conditions reflect tighter vertex-edge consistency.

Example 6. *Consider the universe $\aleph = \{\varphi_1, \varphi_2, \varphi_3, \varphi_4\}$ with parameter $q = 2$. The membership values assigned to vertices are as follows:*

$$\Upsilon(\varphi_1) = \langle 0.9, 0.2, 0.1\rangle, \quad \Upsilon(\varphi_2) = \langle 0.8, 0.3, 0.1\rangle,$$
$$\Upsilon(\varphi_3) = \langle 0.7, 0.2, 0.2\rangle, \quad \Upsilon(\varphi_4) = \langle 0.6, 0.3, 0.2\rangle.$$

The supporting crisp graph is taken as the complete graph K_4 (depicted in Figure 4).

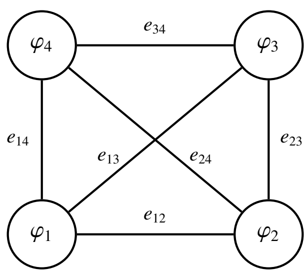

Figure 4. Common structure for all q-ROSFRG types (K_4).

Below, we present four distinct instantiations satisfying the following definitions:

Strong q-ROSFRG:

$$\begin{aligned}
\Delta(\varphi_1\varphi_2) &= \langle 0.8, 0.2, 0.1\rangle, \quad \Delta(\varphi_2\varphi_3) = \langle 0.7, 0.2, 0.2\rangle,\\
\Delta(\varphi_3\varphi_4) &= \langle 0.6, 0.2, 0.2\rangle, \quad \Delta(\varphi_1\varphi_4) = \langle 0.6, 0.2, 0.2\rangle,\\
\Delta(\varphi_1\varphi_3) &= \langle 0.7, 0.2, 0.2\rangle, \quad \Delta(\varphi_2\varphi_4) = \langle 0.6, 0.3, 0.2\rangle.
\end{aligned}$$

Positive membership-strong q-ROSFRG:

$$\begin{aligned}
\Delta(\varphi_1\varphi_2) &= \langle 0.8, 0.1, 0.0\rangle, \quad \Delta(\varphi_2\varphi_3) = \langle 0.7, 0.1, 0.1\rangle,\\
\Delta(\varphi_3\varphi_4) &= \langle 0.6, 0.1, 0.1\rangle, \quad \Delta(\varphi_1\varphi_3) = \langle 0.7, 0.1, 0.1\rangle,\\
\Delta(\varphi_1\varphi_4) &= \langle 0.6, 0.1, 0.1\rangle, \quad \Delta(\varphi_2\varphi_4) = \langle 0.6, 0.1, 0.1\rangle.
\end{aligned}$$

Negative membership-strong q-ROSFRG:

$$\begin{aligned}
\Delta(\varphi_1\varphi_2) &= \langle 0.6, 0.1, 0.1\rangle, \quad \Delta(\varphi_2\varphi_3) = \langle 0.5, 0.1, 0.2\rangle,\\
\Delta(\varphi_3\varphi_4) &= \langle 0.4, 0.1, 0.2\rangle, \quad \Delta(\varphi_1\varphi_4) = \langle 0.5, 0.1, 0.2\rangle,\\
\Delta(\varphi_1\varphi_3) &= \langle 0.5, 0.1, 0.2\rangle, \quad \Delta(\varphi_2\varphi_4) = \langle 0.4, 0.1, 0.2\rangle.
\end{aligned}$$

Complete q-ROSFRG: This case follows the strong pattern but includes all possible adjacency requirements.

Table 3. Comparison of edge membership for $\varphi_1\varphi_2$.

Type	ς	ϱ	$\varkappa$
Strong	0.8	0.2	0.1
Pos-strong	0.8	0.1	0.0
Negm-strong	0.6	0.1	0.1
Complete	0.8	0.2	0.1

The above demonstration shows that distinct edge constraints produce different q-ROSFRG types while keeping the vertex information unchanged.

Definition 12. *Suppose $\mathscr{G}_1 = (\underline{\mathfrak{B}}_1, \overline{\mathfrak{B}}_1)$ and $\mathscr{G}_2 = (\underline{\mathfrak{B}}_2, \overline{\mathfrak{B}}_2)$ are two q-ROSFRGs sharing the same approximation space $(\aleph, \simeq)$ and the same underlying crisp graph $\mathscr{G}^* = (\aleph, \ell)$. For any vertex $\varphi \in \aleph$, we write:*

$$\underline{\mathfrak{B}}_1(\varphi) = (\underline{\mathfrak{B}}_{1\varsigma}(\varphi), \underline{\mathfrak{B}}_{1\varrho}(\varphi), \underline{\mathfrak{B}}_{1\varkappa}(\varphi)), \quad \underline{\mathfrak{B}}_2(\varphi) = (\underline{\mathfrak{B}}_{2\varsigma}(\varphi), \underline{\mathfrak{B}}_{2\varrho}(\varphi), \underline{\mathfrak{B}}_{2\varkappa}(\varphi)),$$

$$\overline{\mathfrak{B}}_1(\varphi) = (\overline{\mathfrak{B}}_{1\varsigma}(\varphi), \overline{\mathfrak{B}}_{1\varrho}(\varphi), \overline{\mathfrak{B}}_{1\varkappa}(\varphi)), \quad \overline{\mathfrak{B}}_2(\varphi) = (\overline{\mathfrak{B}}_{2\varsigma}(\varphi), \overline{\mathfrak{B}}_{2\varrho}(\varphi), \overline{\mathfrak{B}}_{2\varkappa}(\varphi)),$$

where each membership triple respects the q-rung spherical constraint. We now introduce two basic algebraic operations.

(1) Addition ($\oplus$):

$$\underline{\mathfrak{V}}_1 \oplus \underline{\mathfrak{V}}_2(\varphi) = \Big\langle \Big((\underline{\mathfrak{V}}_{1\varsigma}(\varphi))^q + (\underline{\mathfrak{V}}_{2\varsigma}(\varphi))^q - (\underline{\mathfrak{V}}_{1\varsigma}(\varphi) \cdot \underline{\mathfrak{V}}_{2\varsigma}(\varphi))^q \Big)^{1/q}, \underline{\mathfrak{V}}_{1\varrho}(\varphi) \cdot \underline{\mathfrak{V}}_{2\varrho}(\varphi), \\ \Big((\underline{\mathfrak{V}}_{1\varkappa}(\varphi))^q + (\underline{\mathfrak{V}}_{2\varkappa}(\varphi))^q - (\underline{\mathfrak{V}}_{1\varkappa}(\varphi) \cdot \underline{\mathfrak{V}}_{2\varkappa}(\varphi))^q \Big)^{1/q} \Big\rangle, \tag{3.4}$$

with $\overline{\mathfrak{V}}_1 \oplus \overline{\mathfrak{V}}_2(\varphi)$ defined in the same way.

(2) Multiplication ($\otimes$):

$$\underline{\mathfrak{V}}_1 \otimes \underline{\mathfrak{V}}_2(\varphi) = \Big\langle \underline{\mathfrak{V}}_{1\varsigma}(\varphi) \cdot \underline{\mathfrak{V}}_{2\varsigma}(\varphi), \Big((\underline{\mathfrak{V}}_{1\varrho}(\varphi))^q + (\underline{\mathfrak{V}}_{2\varrho}(\varphi))^q - (\underline{\mathfrak{V}}_{1\varrho}(\varphi) \cdot \underline{\mathfrak{V}}_{2\varrho}(\varphi))^q \Big)^{1/q}, \\ \Big((\underline{\mathfrak{V}}_{1\varkappa}(\varphi))^q + (\underline{\mathfrak{V}}_{2\varkappa}(\varphi))^q - (\underline{\mathfrak{V}}_{1\varkappa}(\varphi) \cdot \underline{\mathfrak{V}}_{2\varkappa}(\varphi))^q \Big)^{1/q} \Big\rangle, \tag{3.5}$$

and similarly for $\overline{\mathfrak{V}}_1 \otimes \overline{\mathfrak{V}}_2(\varphi)$.

(3) Edge-based operations: For each edge $\omega\wp \in \ell$, the same formulas apply after replacing the vertex memberships with edge memberships. As an illustration, addition on the edges is given by

$$\underline{\mathfrak{E}}_1 \oplus \underline{\mathfrak{E}}_2(\omega\wp) = \Big\langle \Big((\underline{\mathfrak{E}}_{1\varsigma}(\omega\wp))^q + (\underline{\mathfrak{E}}_{2\varsigma}(\omega\wp))^q - (\underline{\mathfrak{E}}_{1\varsigma}(\omega\wp) \cdot \underline{\mathfrak{E}}_{2\varsigma}(\omega\wp))^q \Big)^{1/q}, \underline{\mathfrak{E}}_{1\varrho}(\omega\wp) \cdot \underline{\mathfrak{E}}_{2\varrho}(\omega\wp), \\ \Big((\underline{\mathfrak{E}}_{1\varkappa}(\omega\wp))^q + (\underline{\mathfrak{E}}_{2\varkappa}(\omega\wp))^q - (\underline{\mathfrak{E}}_{1\varkappa}(\omega\wp) \cdot \underline{\mathfrak{E}}_{2\varkappa}(\omega\wp))^q \Big)^{1/q} \Big\rangle, \tag{3.6}$$

with $\overline{\mathfrak{E}}_1 \oplus \overline{\mathfrak{E}}_2(\omega\wp)$ defined analogously. The multiplication operation $\otimes$ on the edges follows the same pattern as in the vertex case.

Remark 2. *These operations are well-defined only when $\mathscr{G}_1$ and $\mathscr{G}_2$ share the same underlying crisp graph $\mathscr{G}^* = (\aleph, \ell)$. For edges present in only one graph, we extend the other graph's edge membership to $\langle 0, 0, 1\rangle$ (the zero element for a q-ROSFS).*

Definition 13. *Let $\mathscr{G}_1 = (\Upsilon_1, \Delta_1)$ and $\mathscr{G}_2 = (\Upsilon_2, \Delta_2)$ be two q-ROSFRGs with the underlying crisp graphs $\mathscr{G}_1^* = (\aleph_1, \ell_1)$ and $\mathscr{G}_2^* = (\aleph_2, \ell_2)$, respectively. Their Cartesian product is denoted $\mathscr{G}_1 \times \mathscr{G}_2 = (\Upsilon_1 \times \Upsilon_2, \Delta_\times)$, where the vertex membership is given by*

$$\begin{aligned} \varsigma_{\Upsilon_1\times\Upsilon_2}(\varphi_1, \varphi_2) &= \min(\varsigma_{\Upsilon_1}(\varphi_1), \varsigma_{\Upsilon_2}(\varphi_2)), \\ \varrho_{\Upsilon_1\times\Upsilon_2}(\varphi_1, \varphi_2) &= \min(\varrho_{\Upsilon_1}(\varphi_1), \varrho_{\Upsilon_2}(\varphi_2)), \\ \varkappa_{\Upsilon_1\times\Upsilon_2}(\varphi_1, \varphi_2) &= \max(\varkappa_{\Upsilon_1}(\varphi_1), \varkappa_{\Upsilon_2}(\varphi_2)). \end{aligned}$$

For any two vertices (φ_1, φ_2) and (φ_3, φ_4) in the product, the edge memberships are specified as follows:

$$\varsigma_{\Delta_\times}((\varphi_1, \varphi_2)(\varphi_3, \varphi_4)) = \begin{cases} \min(\varsigma_{\Upsilon_1}(\varphi_1), \varsigma_{\Delta_2}(\varphi_2\varphi_4)), & \varphi_1 = \varphi_3,\ \varphi_2\varphi_4 \in \ell_2, \\ \min(\varsigma_{\Delta_1}(\varphi_1\varphi_3), \varsigma_{\Upsilon_2}(\varphi_2)), & \varphi_2 = \varphi_4,\ \varphi_1\varphi_3 \in \ell_1, \\ 0, & \textit{else}. \end{cases}$$

$$\varrho_{\Delta_\times}((\varphi_1,\varphi_2)(\varphi_3,\varphi_4)) = \begin{cases} \min\left(\varrho_{\Upsilon_1}(\varphi_1), \varrho_{\Delta_2}(\varphi_2\varphi_4)\right), & \varphi_1 = \varphi_3,\ \varphi_2\varphi_4 \in \ell_2, \\ \min\left(\varrho_{\Delta_1}(\varphi_1\varphi_3), \varrho_{\Upsilon_2}(\varphi_2)\right), & \varphi_2 = \varphi_4,\ \varphi_1\varphi_3 \in \ell_1, \\ 0, & else. \end{cases}$$

$$\varkappa_{\Delta_\times}((\varphi_1,\varphi_2)(\varphi_3,\varphi_4)) = \begin{cases} \max\left(\varkappa_{\Upsilon_1}(\varphi_1), \varkappa_{\Delta_2}(\varphi_2\varphi_4)\right), & \varphi_1 = \varphi_3,\ \varphi_2\varphi_4 \in \ell_2, \\ \max\left(\varkappa_{\Delta_1}(\varphi_1\varphi_3), \varkappa_{\Upsilon_2}(\varphi_2)\right), & \varphi_2 = \varphi_4,\ \varphi_1\varphi_3 \in \ell_1, \\ 0, & else. \end{cases}$$

Theorem 2. *$\mathscr{G}_1 \times \mathscr{G}_2$ is a q-ROSFRG.*

Proof. For vertices, we have

$$\varsigma^q_{\Upsilon_1\times\Upsilon_2} + \varkappa^q_{\Upsilon_1\times\Upsilon_2} \le \varsigma^q_{\Upsilon_1} + \varkappa^q_{\Upsilon_1} \le 1, \quad \varsigma^q_{\Upsilon_1\times\Upsilon_2} + \varkappa^q_{\Upsilon_1\times\Upsilon_2} \le \varsigma^q_{\Upsilon_2} + \varkappa^q_{\Upsilon_2} \le 1.$$

For edges with $\varphi_1 = \varphi_3$, $\varphi_2\varphi_4 \in \ell_2$, we have

$$\varsigma_{\Delta_\times} = \min(\varsigma_{\Upsilon_1}, \varsigma_{\Delta_2}) \le \min(\varsigma_{\Upsilon_1}, \varsigma_{\Upsilon_2}(\varphi_2), \varsigma_{\Upsilon_2}(\varphi_4)) = \min(\varsigma_{\Upsilon_1\times\Upsilon_2}(\varphi_1,\varphi_2), \varsigma_{\Upsilon_1\times\Upsilon_2}(\varphi_1,\varphi_4)).$$

The case is similar for ϱ and $\varkappa$. The q-rung condition is

$$\varsigma^q_{\Delta_\times} + \varkappa^q_{\Delta_\times} \le \min(\varsigma_1,\varsigma_2)^q + \max(\varkappa_1,\varkappa_2)^q \le 1.$$

Thus, $\mathscr{G}_1 \times \mathscr{G}_2$ is a valid q-ROSFRG. □

Definition 14. *Let $\Theta = \langle \varsigma, \varrho, \varkappa \rangle$ be any q-ROSFS value. We introduce two evaluation functions: The score function $\mathcal{S}$ and the accuracy function $\mathcal{H}$, both mapping from the q-ROSFS to $[0,1]$, defined as*

$$\mathcal{S}(\Theta) = \frac{1 + \varsigma^q - \varkappa^q}{2}, \qquad \mathcal{H}(\Theta) = \varsigma^q + \varrho^q + \varkappa^q.$$

Given two q-ROSFS values Θ and Φ, we establish the total order as follows:

$$\Theta \succ \Phi \Longleftrightarrow \begin{cases} \mathcal{S}(\Theta) > \mathcal{S}(\Phi), & or \\ \mathcal{S}(\Theta) = \mathcal{S}(\Phi) \ \ and \ \ \mathcal{H}(\Theta) > \mathcal{H}(\Phi). \end{cases}$$

The notation $\Theta \succeq \Phi$ means that either $\Theta \succ \Phi$ holds, or Θ and Φ are identical component-wise.

Remark 3. *The score function $\mathcal{S}$ satisfies $0 \le \mathcal{S}(\Theta) \le 1$ since $0 \le \varsigma^q \le 1$ and $0 \le \varkappa^q \le 1$. For a q-ROFS (where $\varrho = 0$), this reduces to the classical q-ROF score function. For a Spherical fuzzy set ($q = 2$), the score function becomes $\mathcal{S} = (1 + \varsigma^2 - \varkappa^2)/2$.*

Proposition 1. *For any q-ROSFS value $\Theta = \langle \varsigma, \varrho, \varkappa \rangle$ with the complement $\Theta^c = \langle \varkappa, \varrho, \varsigma \rangle$, we have*

$$\mathcal{S}(\Theta^c) = 1 - \mathcal{S}(\Theta).$$

Proof. Starting from the definition of the score function, for the complement $\Theta^c = \langle \varkappa, \varrho, \varsigma \rangle$, we obtain

$$\mathcal{S}(\Theta^c) = \frac{1 + (\varkappa)^q - (\varsigma)^q}{2}.$$

This can be rearranged as

$$\mathcal{S}(\Theta^c) = \frac{1 - (\varsigma^q - \varkappa^q)}{2} = \frac{1}{2} - \frac{\varsigma^q - \varkappa^q}{2}.$$

Observe that

$$1 - \mathcal{S}(\Theta) = 1 - \frac{1 + \varsigma^q - \varkappa^q}{2} = \frac{2 - 1 - \varsigma^q + \varkappa^q}{2} = \frac{1 - \varsigma^q + \varkappa^q}{2}.$$

Consequently, we have

$$\mathcal{S}(\Theta^c) = \frac{1 - (\varsigma^q - \varkappa^q)}{2} = \frac{1 - \varsigma^q + \varkappa^q}{2} = 1 - \mathcal{S}(\Theta).$$

This completes the proof. □

Definition 15. *Let $\mathcal{G} = (\underline{\mathfrak{V}}, \overline{\mathfrak{V}})$ be a q-ROSFRG over the crisp graph $\mathcal{G}^* = (\aleph, \ell)$. For any vertex $\varphi \in \aleph$, we define its degree within the lower approximation $\underline{\mathfrak{V}}$ as the triple*

$$\delta_{\underline{\mathfrak{V}}}(\varphi) = \left\langle d_{\underline{\mathfrak{V}}_\varsigma}(\varphi),\ d_{\underline{\mathfrak{V}}_\varrho}(\varphi),\ d_{\underline{\mathfrak{V}}_\varkappa}(\varphi) \right\rangle,$$

where each component aggregates the edge memberships incident to φ

$$d_{\underline{\mathfrak{V}}_\varsigma}(\varphi) = \sum_{\substack{\omega \in \aleph \\ \omega\varphi \in \ell}} \underline{\mathfrak{E}}_\varsigma(\omega\varphi), \quad d_{\underline{\mathfrak{V}}_\varrho}(\varphi) = \sum_{\substack{\omega \in \aleph \\ \omega\varphi \in \ell}} \underline{\mathfrak{E}}_\varrho(\omega\varphi), \quad d_{\underline{\mathfrak{V}}_\varkappa}(\varphi) = \sum_{\substack{\omega \in \aleph \\ \omega\varphi \in \ell}} \underline{\mathfrak{E}}_\varkappa(\omega\varphi).$$

The degree in the upper approximation $\overline{\mathfrak{V}}$ is given analogously as follows:

$$\delta_{\overline{\mathfrak{V}}}(\varphi) = \left\langle d_{\overline{\mathfrak{V}}_\varsigma}(\varphi),\ d_{\overline{\mathfrak{V}}_\varrho}(\varphi),\ d_{\overline{\mathfrak{V}}_\varkappa}(\varphi) \right\rangle,$$

with the components computed by replacing $\underline{\mathfrak{E}}$ with $\overline{\mathfrak{E}}$ in the sums above.

Finally, the total degree of φ combines both approximations using the algebraic sum $\oplus$ from Definition 12

$$\delta_{\mathcal{G}}^{total}(\varphi) = \delta_{\underline{\mathfrak{V}}}(\varphi) \oplus \delta_{\overline{\mathfrak{V}}}(\varphi).$$

Definition 16. *We now adapt the score and accuracy functions from Definition 14 to handle the degree values. Given a degree $\delta(\varphi) = \langle d_\varsigma, d_\varrho, d_\varkappa \rangle$, we set*

$$\mathcal{S}(\delta(\varphi)) = \frac{1 + (d_\varsigma)^q - (d_\varkappa)^q}{2}, \qquad \mathcal{H}(\delta(\varphi)) = (d_\varsigma)^q + (d_\varrho)^q + (d_\varkappa)^q.$$

For any two vertices $\varphi_i, \varphi_j \in \aleph$, we state that

$$\delta(\varphi_i) \succ \delta(\varphi_j)$$

whenever:

$$\begin{cases} \mathcal{S}(\delta(\varphi_i)) > \mathcal{S}(\delta(\varphi_j)), & or \\ \mathcal{S}(\delta(\varphi_i)) = \mathcal{S}(\delta(\varphi_j)) \ \ and \ \ \mathcal{H}(\delta(\varphi_i)) > \mathcal{H}(\delta(\varphi_j)). \end{cases}$$

When neither $\delta(\varphi_i) \succ \delta(\varphi_j)$ nor $\delta(\varphi_j) \succ \delta(\varphi_i)$ is true, we say the two degrees are incomparable.

Theorem 3. *Let $\mathscr{G} = (\underline{\mathfrak{V}}, \overline{\mathfrak{V}})$ be a q-ROSFRG. For any vertex $\varphi \in \aleph$, the following properties hold:*

(1) The lower approximation degree never exceeds the upper one in the following component-wise sense:

$$d_{\underline{\mathfrak{V}}_\varsigma}(\varphi) \leq d_{\overline{\mathfrak{V}}_\varsigma}(\varphi), \quad d_{\underline{\mathfrak{V}}_\varrho}(\varphi) \leq d_{\overline{\mathfrak{V}}_\varrho}(\varphi), \quad d_{\underline{\mathfrak{V}}_\varkappa}(\varphi) \geq d_{\overline{\mathfrak{V}}_\varkappa}(\varphi).$$

(2) When $\mathscr{G}$ is definable (meaning $\underline{\mathfrak{T}}(\mathscr{G}) = \overline{\mathfrak{T}}(\mathscr{G})$), we have the equality

$$\delta_{\underline{\mathfrak{V}}}(\varphi) = \delta_{\overline{\mathfrak{V}}}(\varphi).$$

(3) In the special case of a complete q-ROSFRG, the same equality holds for all $\varphi \in \aleph$:

$$\delta_{\underline{\mathfrak{V}}}(\varphi) = \delta_{\overline{\mathfrak{V}}}(\varphi), \quad \forall \varphi \in \aleph.$$

(4) For the score function applied to degrees, we obtain

$$\mathcal{S}(\delta_{\underline{\mathfrak{V}}}(\varphi)) \leq \mathcal{S}(\delta_{\overline{\mathfrak{V}}}(\varphi)).$$

Proof. Claims (1) through (3) are immediate consequences of Definitions 10 and 15. To establish (4), we start with the score expressions

$$\mathcal{S}(\delta_{\underline{\mathfrak{V}}}(\varphi)) = \frac{1 + (d_{\underline{\mathfrak{V}}_\varsigma})^q - (d_{\underline{\mathfrak{V}}_\varkappa})^q}{2}$$

and

$$\mathcal{S}(\delta_{\overline{\mathfrak{V}}}(\varphi)) = \frac{1 + (d_{\overline{\mathfrak{V}}_\varsigma})^q - (d_{\overline{\mathfrak{V}}_\varkappa})^q}{2}.$$

Using the component-wise inequalities from Part (1)

$$d_{\underline{\mathfrak{V}}_\varsigma} \leq d_{\overline{\mathfrak{V}}_\varsigma}, \qquad d_{\underline{\mathfrak{V}}_\varkappa} \geq d_{\overline{\mathfrak{V}}_\varkappa},$$

we directly obtain:

$$\mathcal{S}(\delta_{\underline{\mathfrak{V}}}(\varphi)) \leq \mathcal{S}(\delta_{\overline{\mathfrak{V}}}(\varphi)).$$

This completes the proof. □

Definition 17. *Let $\mathscr{G} = (\underline{\mathfrak{V}}, \overline{\mathfrak{V}})$ be a q-ROSFRG. A path ϖ of length n connecting φ_0 to φ_n in $\underline{\mathfrak{V}}$ consists of distinct vertices $\varphi_0, \varphi_1, \ldots, \varphi_n$ where, for each step $\iota = 1, \ldots, n$, the edge $\varphi_{\iota-1}\varphi_\iota$ must satisfy*

$$\underline{\mathfrak{E}}_\varsigma(\varphi_{\iota-1}\varphi_\iota) > 0, \quad \underline{\mathfrak{E}}_\varrho(\varphi_{\iota-1}\varphi_\iota) \geq 0, \quad \underline{\mathfrak{E}}_\varkappa(\varphi_{\iota-1}\varphi_\iota) < 1.$$

We measure the strength of such a path as follows:

$$\Psi_{\underline{\mathfrak{V}}}(\varpi) = \bigwedge_{\iota=1}^{n} \underline{\mathfrak{E}}_\varsigma(\varphi_{\iota-1}\varphi_\iota),$$

i.e., the minimum positive membership along the path.

For paths within the upper approximation $\overline{\mathfrak{V}}$, the definition carries over directly after substituting $\underline{\mathfrak{E}}_\varsigma$ with $\overline{\mathfrak{E}}_\varsigma$.

Definition 18. *A q-ROSFRG $\mathscr{G} = (\underline{\mathfrak{V}}, \overline{\mathfrak{V}})$ is categorized according to the following criteria:*

(1) Lower connected: For any two distinct vertices $\varphi_i, \varphi_j \in \aleph$, one can find a path ϖ within $\underline{\mathfrak{V}}$ joining φ_i to φ_j whose strength satisfies

$$\Psi_{\underline{\mathfrak{V}}}(\varpi) > 0.$$

(2) Upper connected: For any two distinct vertices $\varphi_i, \varphi_j \in \aleph$, there is a path ϖ within $\overline{\mathfrak{V}}$ connecting φ_i to φ_j with

$$\Psi_{\overline{\mathfrak{V}}}(\varpi) > 0.$$

(3) Connected: The structure is said to be connected whenever both lower and upper connectedness hold simultaneously.

Theorem 4. *Let $\mathscr{G} = (\underline{\mathfrak{V}}, \overline{\mathfrak{V}})$ be a q-ROSFRG. In this case*

$$\textit{Lower connected} \Rightarrow \textit{Connected} \Rightarrow \textit{Upper connected.}$$

Proof. We prove the implications separately.

(1) Assume that $\underline{\mathfrak{V}}$ is lower connected. Then for any $\varphi_i, \varphi_j \in \aleph$, a path $\varpi = \varphi_0, \varphi_1, \ldots, \varphi_n$ exists in $\underline{\mathfrak{V}}$ with $\varphi_0 = \varphi_i$, $\varphi_n = \varphi_j$ and $\Psi_{\underline{\mathfrak{V}}}(\varpi) > 0$. From Definition 10, for any edge $\omega\wp \in \ell$

$$\underline{\mathfrak{E}}_{\varsigma}(\omega\wp) \leq \varsigma_\Delta(\omega\wp), \quad \underline{\mathfrak{E}}_{\varrho}(\omega\wp) \leq \varrho_\Delta(\omega\wp), \quad \underline{\mathfrak{E}}_{\varkappa}(\omega\wp) \geq \varkappa_\Delta(\omega\wp).$$

Hence, $\underline{\mathfrak{E}}_{\varsigma}(\varphi_{\iota-1}\varphi_\iota) > 0 \Rightarrow \varsigma_\Delta(\varphi_{\iota-1}\varphi_\iota) > 0$, so ϖ is also a path in $\mathscr{G}$. Moreover

$$\Psi_{\mathscr{G}}(\varpi) = \bigwedge_{\iota=1}^{n} \varsigma_\Delta(\varphi_{\iota-1}\varphi_\iota) \geq \bigwedge_{\iota=1}^{n} \underline{\mathfrak{E}}_{\varsigma}(\varphi_{\iota-1}\varphi_\iota) = \Psi_{\underline{\mathfrak{V}}}(\varpi) > 0.$$

Thus $\mathscr{G}$ is connected.

(2) Assume that $\mathscr{G}$ is connected. Then for any $\varphi_i, \varphi_j \in \aleph$, a path $\varpi = \varphi_0, \varphi_1, \ldots, \varphi_m$ exists in $\mathscr{G}$ with $\Psi_{\mathscr{G}}(\varpi) > 0$. For each edge $\varphi_{\lambda-1}\varphi_\lambda$

$$\overline{\mathfrak{E}}_{\varsigma}(\varphi_{\lambda-1}\varphi_\lambda) \geq \varsigma_\Delta(\varphi_{\lambda-1}\varphi_\lambda) > 0,$$

so ϖ is also a path in $\overline{\mathfrak{V}}$. Furthermore

$$\Psi_{\overline{\mathfrak{V}}}(\varpi) = \bigwedge_{\lambda=1}^{m} \overline{\mathfrak{E}}_{\varsigma}(\varphi_{\lambda-1}\varphi_\lambda) \geq \bigwedge_{\lambda=1}^{m} \varsigma_\Delta(\varphi_{\lambda-1}\varphi_\lambda) = \Psi_{\mathscr{G}}(\varpi) > 0.$$

Hence, $\overline{\mathfrak{V}}$ is upper connected.

This completes the proof. □

Definition 19. *Let $\mathscr{G}_1 = (\underline{\mathfrak{B}}_1, \overline{\mathfrak{B}}_1)$ and $\mathscr{G}_2 = (\underline{\mathfrak{B}}_2, \overline{\mathfrak{B}}_2)$ be two q-ROSFRGs sharing the same vertex set $\aleph$ with $|\aleph| = n$. We first quantify the resemblance between their lower approximations via the following:*

$$\begin{aligned}\mathfrak{S}_{\underline{\mathfrak{B}}}(\mathscr{G}_1, \mathscr{G}_2) = 1 - \frac{1}{3n(n-1)} \sum_{\substack{\omega,\wp \in \aleph \\ \omega \neq \wp}} \Big(&\left|\underline{\mathfrak{E}}_{1\varsigma}(\omega\wp) - \underline{\mathfrak{E}}_{2\varsigma}(\omega\wp)\right| \\ &+ \left|\underline{\mathfrak{E}}_{1\varrho}(\omega\wp) - \underline{\mathfrak{E}}_{2\varrho}(\omega\wp)\right| \\ &+ \left|\underline{\mathfrak{E}}_{1\varkappa}(\omega\wp) - \underline{\mathfrak{E}}_{2\varkappa}(\omega\wp)\right|\Big).\end{aligned} \tag{3.7}$$

An analogous expression $\mathfrak{S}_{\overline{\mathfrak{B}}}(\mathscr{G}_1, \mathscr{G}_2)$ applies to the upper approximations, replacing $\underline{\mathfrak{E}}$ with $\overline{\mathfrak{E}}$. The overall similarity between $\mathscr{G}_1$ and $\mathscr{G}_2$ is then taken as the average of the two components:

$$\mathfrak{S}_{total}(\mathscr{G}_1, \mathscr{G}_2) = \frac{\mathfrak{S}_{\underline{\mathfrak{B}}}(\mathscr{G}_1, \mathscr{G}_2) + \mathfrak{S}_{\overline{\mathfrak{B}}}(\mathscr{G}_1, \mathscr{G}_2)}{2}.$$

Theorem 5. *The similarity measure $\mathfrak{S}_{\underline{\mathfrak{B}}}$ satisfies the following for all $\mathscr{G}_1, \mathscr{G}_2, \mathscr{G}_3$:*

(1) $0 \leq \mathfrak{S}_{\underline{\mathfrak{B}}}(\mathscr{G}_1, \mathscr{G}_2) \leq 1$.

(2) $\mathfrak{S}_{\underline{\mathfrak{B}}}(\mathscr{G}_1, \mathscr{G}_2) = \mathfrak{S}_{\underline{\mathfrak{B}}}(\mathscr{G}_2, \mathscr{G}_1)$.

(3) $\mathfrak{S}_{\underline{\mathfrak{B}}}(\mathscr{G}_1, \mathscr{G}_1) = 1$.

(4) $\mathfrak{S}_{\underline{\mathfrak{B}}}(\mathscr{G}_1, \mathscr{G}_2) = 1$ *if and only if* $\underline{\mathfrak{B}}_{1\varsigma}(\omega\wp) = \underline{\mathfrak{B}}_{2\varsigma}(\omega\wp)$ *for all* $\omega\wp \in \ell$.

(5) $d(\mathscr{G}_1, \mathscr{G}_3) \leq d(\mathscr{G}_1, \mathscr{G}_2) + d(\mathscr{G}_2, \mathscr{G}_3)$, *where* $d = 1 - \mathfrak{S}_{\underline{\mathfrak{B}}}$.

Proof. We establish each claim systematically.

(1) Because all membership values lie in $[0, 1]$, each absolute difference satisfies $0 \leq |x - y| \leq 1$. Consequently, we have

$$\begin{aligned} 0 &\leq |\underline{\mathfrak{E}}_{1\varsigma}(\omega\wp) - \underline{\mathfrak{E}}_{2\varsigma}(\omega\wp)| \leq 1, \\ 0 &\leq |\underline{\mathfrak{E}}_{1\varrho}(\omega\wp) - \underline{\mathfrak{E}}_{2\varrho}(\omega\wp)| \leq 1, \\ 0 &\leq |\underline{\mathfrak{E}}_{1\varkappa}(\omega\wp) - \underline{\mathfrak{E}}_{2\varkappa}(\omega\wp)| \leq 1. \end{aligned}$$

Aggregating across all unordered vertex pairs and the three components gives

$$0 \leq \sum_{\omega \neq \wp} \left(|\underline{\mathfrak{E}}_{1\varsigma} - \underline{\mathfrak{E}}_{2\varsigma}| + |\underline{\mathfrak{E}}_{1\varrho} - \underline{\mathfrak{E}}_{2\varrho}| + |\underline{\mathfrak{E}}_{1\varkappa} - \underline{\mathfrak{E}}_{2\varkappa}| \right) \leq 3n(n-1).$$

Dividing by $3n(n-1)$ and subtracting from 1 preserves the bounds, hence

$$0 \leq \mathfrak{S}_{\underline{\mathfrak{B}}}(\mathscr{G}_1, \mathscr{G}_2) \leq 1.$$

(2) Symmetry follows immediately from $|a - b| = |b - a|$ for each component. Therefore

$$\mathfrak{S}_{\underline{\mathfrak{B}}}(\mathscr{G}_1, \mathscr{G}_2) = \mathfrak{S}_{\underline{\mathfrak{B}}}(\mathscr{G}_2, \mathscr{G}_1).$$

(3) When $\mathscr{G}_1 = \mathscr{G}_2$, every absolute difference becomes zero, yielding

$$\mathfrak{S}_{\underline{\mathfrak{V}}}(\mathscr{G}_1, \mathscr{G}_1) = 1.$$

(4) Conversely, $\mathfrak{S}_{\underline{\mathfrak{V}}}(\mathscr{G}_1, \mathscr{G}_2) = 1$ forces the normalized sum to vanish, which implies

$$|\underline{\mathfrak{E}}_{1\varsigma} - \underline{\mathfrak{E}}_{2\varsigma}| = |\underline{\mathfrak{E}}_{1\varrho} - \underline{\mathfrak{E}}_{2\varrho}| = |\underline{\mathfrak{E}}_{1\varkappa} - \underline{\mathfrak{E}}_{2\varkappa}| = 0$$

for all edges. Thus the two graphs have identical edge memberships, and the reverse direction is immediate.

(5) Applying the triangle inequality $|a - c| \leq |a - b| + |b - c|$ component-wise gives us

$$\begin{aligned} |\underline{\mathfrak{E}}_{1\varsigma} - \underline{\mathfrak{E}}_{3\varsigma}| &\leq |\underline{\mathfrak{E}}_{1\varsigma} - \underline{\mathfrak{E}}_{2\varsigma}| + |\underline{\mathfrak{E}}_{2\varsigma} - \underline{\mathfrak{E}}_{3\varsigma}|, \\ |\underline{\mathfrak{E}}_{1\varrho} - \underline{\mathfrak{E}}_{3\varrho}| &\leq |\underline{\mathfrak{E}}_{1\varrho} - \underline{\mathfrak{E}}_{2\varrho}| + |\underline{\mathfrak{E}}_{2\varrho} - \underline{\mathfrak{E}}_{3\varrho}|, \\ |\underline{\mathfrak{E}}_{1\varkappa} - \underline{\mathfrak{E}}_{3\varkappa}| &\leq |\underline{\mathfrak{E}}_{1\varkappa} - \underline{\mathfrak{E}}_{2\varkappa}| + |\underline{\mathfrak{E}}_{2\varkappa} - \underline{\mathfrak{E}}_{3\varkappa}|. \end{aligned}$$

Summation over all $\omega \neq \wp$ leads to $D_{13} \leq D_{12} + D_{23}$, where D_{ij} denotes the total absolute difference sum. Consequently, we have

$$\mathfrak{S}_{13} \geq \mathfrak{S}_{12} + \mathfrak{S}_{23} - 1,$$

or equivalently $d_{13} \leq d_{12} + d_{23}$ with $d = 1 - \mathfrak{S}$.

This completes the proof. □

Definition 20. *Let $\mathfrak{Z} = \{\varphi_1, \varphi_2, \ldots, \varphi_n\}$ be a set of crisp numerical values. For a parameter $q \geq 1$, the q-ROSFS fuzzification function $\mathcal{F}: \mathbb{R} \to$ q-ROSFS is defined by:*

$$\mathcal{F}(\varphi_i) = \langle \varsigma_i, \varrho_i, \varkappa_i \rangle,$$

where the positive membership is given by:

$$\varsigma_i = \left(\frac{\varphi_i - \varphi_{\min}}{\varphi_{\max} - \varphi_{\min}} \right)^{1/q}.$$

The neutral and negative memberships are defined as:

$$\varrho_i = \eta \cdot \left(1 - \varsigma_i^q\right)^{1/q}, \quad \varkappa_i = \left(1 - \varsigma_i^q - \varrho_i^q\right)^{1/q}.$$

Here, $\eta \in (0, 1)$ is a fixed neutral factor (typically $\eta = 0.1$), and $\varphi_{\min} = \min_i \varphi_i$, $\varphi_{\max} = \max_i \varphi_i$. For expert-based evaluations, each expert directly provides a triplet $(\varsigma, \varrho, \varkappa)$ satisfying:

$$\varsigma^q + \varrho^q + \varkappa^q \leq 1.$$

Theorem 6. *The fuzzification function $\mathcal{F}$ defined in Definition 20 produces valid q-ROSFS values, i.e., for each φ_i, we have*

$$\varsigma_i^q + \varrho_i^q + \varkappa_i^q \leq 1.$$

Proof. We verify the condition by direct computation.

Let
$$t_i = \frac{\varphi_i - \varphi_{\min}}{\varphi_{\max} - \varphi_{\min}} \in [0, 1],$$
so that
$$\varsigma_i^q = t_i.$$
Then:
$$\varrho_i^q = \eta^q(1 - \varsigma_i^q) = \eta^q(1 - t_i)$$
and
$$\varkappa_i^q = 1 - \varsigma_i^q - \varrho_i^q = 1 - t_i - \eta^q(1 - t_i) = (1 - t_i)(1 - \eta^q).$$
Now,
$$\begin{aligned} \varsigma_i^q + \varrho_i^q + \varkappa_i^q &= t_i + \eta^q(1 - t_i) + (1 - t_i)(1 - \eta^q) \\ &= t_i + (1 - t_i)(\eta^q + 1 - \eta^q) \\ &= t_i + (1 - t_i) = 1. \end{aligned}$$
Hence, the q-rung spherical condition holds with equality, and $\mathscr{F}(\varphi_i)$ is a valid q-ROSFS value. □

Theorem 7. *Let $\mathscr{G} = (\Upsilon, \Delta)$ be a q-ROSFRG constructed over the approximation space $(\aleph, \simeq)$, where $\simeq$ forms an equivalence relation on $\aleph$. Then the following idempotency properties hold:*
$$\underline{\mathfrak{T}}(\underline{\mathfrak{T}}(\mathscr{G})) = \underline{\mathfrak{T}}(\mathscr{G}), \quad \overline{\mathfrak{T}}(\overline{\mathfrak{T}}(\mathscr{G})) = \overline{\mathfrak{T}}(\mathscr{G}).$$

Proof. We focus on the lower approximation operator; the upper approximation case follows by duality (swapping $\bigwedge$ with $\bigvee$).

(1) Vertex component: fix an arbitrary $\varphi \in \aleph$. By definition, we have
$$\underline{\mathfrak{B}}_{\varsigma\underline{\mathfrak{T}}(\mathscr{G})}(\varphi) = \bigwedge_{\omega\in[\varphi]_\simeq} \underline{\mathfrak{B}}_{\varsigma\mathscr{G}}(\omega).$$
Recall that for any $\omega \in [\varphi]_\simeq$, we have
$$\underline{\mathfrak{B}}_{\varsigma\mathscr{G}}(\omega) = \bigwedge_{\wp\in[\omega]_\simeq} \varsigma_\Upsilon(\wp).$$
Since $\simeq$ is an equivalence relation, $[\omega]_\simeq = [\varphi]_\simeq$. Substituting, we have
$$\underline{\mathfrak{B}}_{\varsigma\underline{\mathfrak{T}}(\mathscr{G})}(\varphi) = \bigwedge_{\omega\in[\varphi]_\simeq} \left(\bigwedge_{\wp\in[\varphi]_\simeq} \varsigma_\Upsilon(\wp) \right) = \bigwedge_{\wp\in[\varphi]_\simeq} \varsigma_\Upsilon(\wp) = \underline{\mathfrak{B}}_{\varsigma\mathscr{G}}(\varphi).$$
An identical computation for the neutral component gives
$$\underline{\mathfrak{B}}_{\varrho\underline{\mathfrak{T}}(\mathscr{G})}(\varphi) = \bigwedge_{\omega\in[\varphi]_\simeq} \underline{\mathfrak{B}}_{\varrho\mathscr{G}}(\omega) = \underline{\mathfrak{B}}_{\varrho\mathscr{G}}(\varphi),$$
while, for the negative component (where the operation switches to $\bigvee$), we have
$$\underline{\mathfrak{B}}_{\varkappa\underline{\mathfrak{T}}(\mathscr{G})}(\varphi) = \bigvee_{\omega\in[\varphi]_\simeq} \underline{\mathfrak{B}}_{\varkappa\mathscr{G}}(\omega) = \underline{\mathfrak{B}}_{\varkappa\mathscr{G}}(\varphi).$$
Thus $\underline{\mathfrak{T}}(\underline{\mathfrak{T}}(\mathscr{G}))(\varphi) = \underline{\mathfrak{T}}(\mathscr{G})(\varphi)$ holds for all vertices.

(2) Edge component: now take any edge $\omega\wp \in \ell$. In this case

$$\underline{\mathfrak{E}}_{\varsigma\underline{\mathfrak{T}}(\Delta)}(\omega\wp) = \bigwedge_{\varphi\in[\omega]_{\simeq}} \bigwedge_{\varphi'\in[\wp]_{\simeq}} \underline{\mathfrak{E}}_{\varsigma\Delta}(\varphi\varphi').$$

For $\underline{\mathfrak{E}}_{\varsigma\Delta}(\varphi\varphi')$, we have

$$\underline{\mathfrak{E}}_{\varsigma\Delta}(\varphi\varphi') = \bigwedge_{\varphi''\in[\varphi]_{\simeq}} \bigwedge_{\varphi'''\in[\varphi']_{\simeq}} \varsigma_{\Delta}(\varphi''\varphi''').$$

Because $[\varphi]_{\simeq} = [\omega]_{\simeq}$ and $[\varphi']_{\simeq} = [\wp]_{\simeq}$

$$\underline{\mathfrak{E}}_{\varsigma\underline{\mathfrak{T}}(\Delta)}(\omega\wp) = \bigwedge_{\varphi''\in[\omega]_{\simeq}} \bigwedge_{\varphi'''\in[\wp]_{\simeq}} \varsigma_{\Delta}(\varphi''\varphi''') = \underline{\mathfrak{E}}_{\varsigma\Delta}(\omega\wp).$$

The same reasoning applies to the neutral and negative components without modification.

Consequently, $\underline{\mathfrak{T}}(\underline{\mathfrak{T}}(\mathscr{G})) = \underline{\mathfrak{T}}(\mathscr{G})$. The statement for the upper approximation follows by applying the same steps with $\bigwedge$ and $\bigvee$ interchanged throughout. $\square$

Definition 21. *Let* $\mathscr{G}_1 = (\underline{\mathfrak{B}}_1, \overline{\mathfrak{B}}_1)$ *and* $\mathscr{G}_2 = (\underline{\mathfrak{B}}_2, \overline{\mathfrak{B}}_2)$ *be two q-ROSFRGs sharing the same vertex set* $\aleph$*, the equivalence relation* $\simeq$*, and the underlying crisp graph* $\mathscr{G}^* = (\aleph, \ell)$*.*

Union operation ($\mathscr{G}_1 \cup \mathscr{G}_2$)*: defined component-wise as* ($\underline{\mathfrak{B}}_1 \cup \underline{\mathfrak{B}}_2$, $\overline{\mathfrak{B}}_1 \cup \overline{\mathfrak{B}}_2$)*, where for each vertex* $\varphi \in \aleph$*, we have*

$$(\underline{\mathfrak{B}}_1 \cup \underline{\mathfrak{B}}_2)(\varphi) = \left\langle \underline{\mathfrak{B}}_{1\varsigma}(\varphi) \vee \underline{\mathfrak{B}}_{2\varsigma}(\varphi),\ \underline{\mathfrak{B}}_{1\varrho}(\varphi) \wedge \underline{\mathfrak{B}}_{2\varrho}(\varphi),\ \underline{\mathfrak{B}}_{1\varkappa}(\varphi) \wedge \underline{\mathfrak{B}}_{2\varkappa}(\varphi) \right\rangle,$$

$$(\overline{\mathfrak{B}}_1 \cup \overline{\mathfrak{B}}_2)(\varphi) = \left\langle \overline{\mathfrak{B}}_{1\varsigma}(\varphi) \vee \overline{\mathfrak{B}}_{2\varsigma}(\varphi),\ \overline{\mathfrak{B}}_{1\varrho}(\varphi) \wedge \overline{\mathfrak{B}}_{2\varrho}(\varphi),\ \overline{\mathfrak{B}}_{1\varkappa}(\varphi) \wedge \overline{\mathfrak{B}}_{2\varkappa}(\varphi) \right\rangle.$$

Intersection operation ($\mathscr{G}_1 \cap \mathscr{G}_2$)*: given by* ($\underline{\mathfrak{B}}_1 \cap \underline{\mathfrak{B}}_2$, $\overline{\mathfrak{B}}_1 \cap \overline{\mathfrak{B}}_2$) *with:*

$$(\underline{\mathfrak{B}}_1 \cap \underline{\mathfrak{B}}_2)(\varphi) = \left\langle \underline{\mathfrak{B}}_{1\varsigma}(\varphi) \wedge \underline{\mathfrak{B}}_{2\varsigma}(\varphi),\ \underline{\mathfrak{B}}_{1\varrho}(\varphi) \vee \underline{\mathfrak{B}}_{2\varrho}(\varphi),\ \underline{\mathfrak{B}}_{1\varkappa}(\varphi) \vee \underline{\mathfrak{B}}_{2\varkappa}(\varphi) \right\rangle,$$

$$(\overline{\mathfrak{B}}_1 \cap \overline{\mathfrak{B}}_2)(\varphi) = \left\langle \overline{\mathfrak{B}}_{1\varsigma}(\varphi) \wedge \overline{\mathfrak{B}}_{2\varsigma}(\varphi),\ \overline{\mathfrak{B}}_{1\varrho}(\varphi) \vee \overline{\mathfrak{B}}_{2\varrho}(\varphi),\ \overline{\mathfrak{B}}_{1\varkappa}(\varphi) \vee \overline{\mathfrak{B}}_{2\varkappa}(\varphi) \right\rangle.$$

For the edges $\omega\wp \in \ell$*, the same formulas apply after substituting the edge membership functions* ($\underline{\mathfrak{E}}$, $\overline{\mathfrak{E}}$) *in place of the vertex memberships.*

Theorem 8. *If* $\mathscr{G}_1$ *and* $\mathscr{G}_2$ *are q-ROSFRGs, then both* $\mathscr{G}_1 \cup \mathscr{G}_2$ *and* $\mathscr{G}_1 \cap \mathscr{G}_2$ *are also q-ROSFRGs. Additionally, the following relationships hold:*

(1) $\underline{\mathfrak{T}}(\mathscr{G}_1 \cup \mathscr{G}_2) = \underline{\mathfrak{T}}(\mathscr{G}_1) \cup \underline{\mathfrak{T}}(\mathscr{G}_2)$.

(2) $\overline{\mathfrak{T}}(\mathscr{G}_1 \cap \mathscr{G}_2) = \overline{\mathfrak{T}}(\mathscr{G}_1) \cap \overline{\mathfrak{T}}(\mathscr{G}_2)$.

(3) $\underline{\mathfrak{T}}(\mathscr{G}_1 \cap \mathscr{G}_2) \subseteq \underline{\mathfrak{T}}(\mathscr{G}_1) \cap \underline{\mathfrak{T}}(\mathscr{G}_2)$.

(4) $\overline{\mathfrak{T}}(\mathscr{G}_1 \cup \mathscr{G}_2) \supseteq \overline{\mathfrak{T}}(\mathscr{G}_1) \cup \overline{\mathfrak{T}}(\mathscr{G}_2)$.

Proof. We begin by verifying that $\underline{\mathfrak{V}}_1 \cup \underline{\mathfrak{V}}_2$ satisfies the q-rung spherical condition; the other operations follow the same reasoning.

Take any $\varphi \in \aleph$ and set

$$p = \underline{\mathfrak{V}}_{1\varsigma}(\varphi) \vee \underline{\mathfrak{V}}_{2\varsigma}(\varphi), \quad n = \underline{\mathfrak{V}}_{1\varrho}(\varphi) \wedge \underline{\mathfrak{V}}_{2\varrho}(\varphi), \quad m = \underline{\mathfrak{V}}_{1\varkappa}(\varphi) \wedge \underline{\mathfrak{V}}_{2\varkappa}(\varphi).$$

Because both $\mathscr{G}_1$ and $\mathscr{G}_2$ are valid q-ROSFRGs, we have

$$\underline{\mathfrak{V}}_{1\varsigma}(\varphi)^q + \underline{\mathfrak{V}}_{1\varrho}(\varphi)^q + \underline{\mathfrak{V}}_{1\varkappa}(\varphi)^q \leq 1, \qquad \underline{\mathfrak{V}}_{2\varsigma}(\varphi)^q + \underline{\mathfrak{V}}_{2\varrho}(\varphi)^q + \underline{\mathfrak{V}}_{2\varkappa}(\varphi)^q \leq 1.$$

We need to establish $p^q + n^q + m^q \leq 1$. Notice that

$$p^q = \max(\underline{\mathfrak{V}}_{1\varsigma}(\varphi)^q, \underline{\mathfrak{V}}_{2\varsigma}(\varphi)^q), \quad n^q = \min(\underline{\mathfrak{V}}_{1\varrho}(\varphi)^q, \underline{\mathfrak{V}}_{2\varrho}(\varphi)^q), \quad m^q = \min(\underline{\mathfrak{V}}_{1\varkappa}(\varphi)^q, \underline{\mathfrak{V}}_{2\varkappa}(\varphi)^q).$$

For brevity, write $a_i = \underline{\mathfrak{V}}_{i\varsigma}(\varphi)^q$, $b_i = \underline{\mathfrak{V}}_{i\varrho}(\varphi)^q$, and $c_i = \underline{\mathfrak{V}}_{i\varkappa}(\varphi)^q$. We then have

$$p^q + n^q + m^q = \max(a_1, a_2) + \min(b_1, b_2) + \min(c_1, c_2).$$

Without loss of generality, suppose that $a_1 \geq a_2$, so $\max(a_1, a_2) = a_1$. We examine the four possible orderings of b_1, b_2 and c_1, c_2.

- If $b_1 \leq b_2$ and $c_1 \leq c_2$: The sum becomes $a_1 + b_1 + c_1 \leq 1$.
- If $b_1 \leq b_2$ and $c_2 \leq c_1$: The sum becomes $a_1 + b_1 + c_2 \leq 1$.
- If $b_2 \leq b_1$ and $c_1 \leq c_2$: The sum becomes $a_1 + b_2 + c_1 \leq 1$.
- If $b_2 \leq b_1$ and $c_2 \leq c_1$: The sum becomes $a_1 + b_2 + c_2 \leq 1$.

In every scenario, the total does not exceed 1, confirming that $\underline{\mathfrak{V}}_1 \cup \underline{\mathfrak{V}}_2$ is valid. The remaining validity statements are proved analogously.

We now turn to Properties 1–4.

(1)

$$\begin{aligned}
\underline{\mathfrak{V}}_{\varsigma\underline{\mathfrak{T}}(\mathscr{G}_1 \cup \mathscr{G}_2)}(\varphi) &= \bigwedge_{\omega \in [\varphi]_{\simeq}} (\underline{\mathfrak{V}}_{1\varsigma}(\omega) \vee \underline{\mathfrak{V}}_{2\varsigma}(\omega)) \\
&= \left(\bigwedge_{\omega \in [\varphi]_{\simeq}} \underline{\mathfrak{V}}_{1\varsigma}(\omega) \right) \vee \left(\bigwedge_{\omega \in [\varphi]_{\simeq}} \underline{\mathfrak{V}}_{2\varsigma}(\omega) \right) \\
&= \underline{\mathfrak{V}}_{\varsigma\mathscr{G}_1}(\varphi) \vee \underline{\mathfrak{V}}_{\varsigma\mathscr{G}_2}(\varphi).
\end{aligned}$$

The case is similar for $\underline{\mathfrak{V}}_{\varrho}$ and $\underline{\mathfrak{V}}_{\varkappa}$.

(2)

$$\begin{aligned}
\overline{\mathfrak{V}}_{\varsigma\overline{\mathfrak{T}}(\mathscr{G}_1 \cap \mathscr{G}_2)}(\varphi) &= \bigvee_{\omega \in [\varphi]_{\simeq}} (\overline{\mathfrak{V}}_{1\varsigma}(\omega) \wedge \overline{\mathfrak{V}}_{2\varsigma}(\omega)) \\
&= \left(\bigvee_{\omega \in [\varphi]_{\simeq}} \overline{\mathfrak{V}}_{1\varsigma}(\omega) \right) \wedge \left(\bigvee_{\omega \in [\varphi]_{\simeq}} \overline{\mathfrak{V}}_{2\varsigma}(\omega) \right) \\
&= \overline{\mathfrak{V}}_{\varsigma\mathscr{G}_1}(\varphi) \wedge \overline{\mathfrak{V}}_{\varsigma\mathscr{G}_2}(\varphi).
\end{aligned}$$

(3) Using $\mathscr{G}_1 \cap \mathscr{G}_2 \subseteq \mathscr{G}_i$, we have

$$\underline{\mathfrak{T}}(\mathscr{G}_1 \cap \mathscr{G}_2) \subseteq \underline{\mathfrak{T}}(\mathscr{G}_1), \quad \underline{\mathfrak{T}}(\mathscr{G}_1 \cap \mathscr{G}_2) \subseteq \underline{\mathfrak{T}}(\mathscr{G}_2).$$

Hence,

$$\underline{\mathfrak{T}}(\mathscr{G}_1 \cap \mathscr{G}_2) \subseteq \underline{\mathfrak{T}}(\mathscr{G}_1) \cap \underline{\mathfrak{T}}(\mathscr{G}_2).$$

(4) Since $\mathscr{G}_i \subseteq \mathscr{G}_1 \cup \mathscr{G}_2$:

$$\overline{\mathfrak{T}}(\mathscr{G}_1) \subseteq \overline{\mathfrak{T}}(\mathscr{G}_1 \cup \mathscr{G}_2), \quad \overline{\mathfrak{T}}(\mathscr{G}_2) \subseteq \overline{\mathfrak{T}}(\mathscr{G}_1 \cup \mathscr{G}_2).$$

Thus,

$$\overline{\mathfrak{T}}(\mathscr{G}_1) \cup \overline{\mathfrak{T}}(\mathscr{G}_2) \subseteq \overline{\mathfrak{T}}(\mathscr{G}_1 \cup \mathscr{G}_2).$$

This completes the proof. □

Definition 22. *Let $\mathscr{G} = (\underline{\mathfrak{B}}, \overline{\mathfrak{B}})$ be a q-ROSFRG. Its complement is denoted*

$$\mathscr{G}^c = (\underline{\mathfrak{B}}^c, \overline{\mathfrak{B}}^c)$$

and defined as follows. For each vertex $\varphi \in \aleph$, we have

$$\underline{\mathfrak{B}}^c(\varphi) = \left\langle \underline{\mathfrak{B}}_{\varkappa\mathscr{G}}(\varphi), \, \underline{\mathfrak{B}}_{\varrho\mathscr{G}}(\varphi), \, \underline{\mathfrak{B}}_{\varsigma\mathscr{G}}(\varphi) \right\rangle, \qquad \overline{\mathfrak{B}}^c(\varphi) = \left\langle \overline{\mathfrak{B}}_{\varkappa\mathscr{G}}(\varphi), \, \overline{\mathfrak{B}}_{\varrho\mathscr{G}}(\varphi), \, \overline{\mathfrak{B}}_{\varsigma\mathscr{G}}(\varphi) \right\rangle.$$

For any edge $\omega\wp \in \ell$, we have

$$\underline{\mathfrak{E}}^c(\omega\wp) = \left\langle \underline{\mathfrak{E}}_{\varkappa\Delta}(\omega\wp), \, \underline{\mathfrak{E}}_{\varrho\Delta}(\omega\wp), \, \underline{\mathfrak{E}}_{\varsigma\Delta}(\omega\wp) \right\rangle, \qquad \overline{\mathfrak{E}}^c(\omega\wp) = \left\langle \overline{\mathfrak{E}}_{\varkappa\Delta}(\omega\wp), \, \overline{\mathfrak{E}}_{\varrho\Delta}(\omega\wp), \, \overline{\mathfrak{E}}_{\varsigma\Delta}(\omega\wp) \right\rangle.$$

Theorem 9. *For any q-ROSFRG $\mathscr{G}$, the complement satisfies the following:*

(1) Involution: $(\mathscr{G}^c)^c = \mathscr{G}$.

(2) $\underline{\mathfrak{T}}(\mathscr{G}^c) = (\overline{\mathfrak{T}}(\mathscr{G}))^c$.

(3) $\overline{\mathfrak{T}}(\mathscr{G}^c) = (\underline{\mathfrak{T}}(\mathscr{G}))^c$.

(4) For any q-ROSFS value $x = \langle \varsigma_x, \varrho_x, \varkappa_x \rangle$ attached to a vertex or edge, $\mathcal{S}(x^c) = 1 - \mathcal{S}(x)$, where $x^c = \langle \varkappa_x, \varrho_x, \varsigma_x \rangle$.

Proof. We verify each statement in order.

(1) Starting from the definition and applying the complement twice, we have

$$\begin{aligned}
\underline{\mathfrak{B}}^{cc}(\varphi) &= \langle \underline{\mathfrak{B}}_{\varsigma\mathscr{G}^c}(\varphi), \underline{\mathfrak{B}}_{\varrho\mathscr{G}^c}(\varphi), \underline{\mathfrak{B}}_{\varkappa\mathscr{G}^c}(\varphi) \rangle^c \\
&= \langle \underline{\mathfrak{B}}_{\varkappa\mathscr{G}}(\varphi), \underline{\mathfrak{B}}_{\varrho\mathscr{G}}(\varphi), \underline{\mathfrak{B}}_{\varsigma\mathscr{G}}(\varphi) \rangle^c \\
&= \langle \underline{\mathfrak{B}}_{\varsigma\mathscr{G}}(\varphi), \underline{\mathfrak{B}}_{\varrho\mathscr{G}}(\varphi), \underline{\mathfrak{B}}_{\varkappa\mathscr{G}}(\varphi) \rangle = \underline{\mathfrak{B}}(\varphi).
\end{aligned}$$

The same computation works for $\overline{\mathfrak{B}}$, yielding

$$(\mathscr{G}^c)^c = \mathscr{G}.$$

(2) For an arbitrary $\varphi \in \aleph$, we have

$$\underline{\mathfrak{T}}(\mathscr{G}^c)(\varphi) = \left\langle \bigwedge_{\omega\in[\varphi]_\simeq} \underline{\mathfrak{B}}_{\varkappa\mathscr{G}}(\omega), \bigwedge_{\omega\in[\varphi]_\simeq} \underline{\mathfrak{B}}_{\varrho\mathscr{G}}(\omega), \bigvee_{\omega\in[\varphi]_\simeq} \underline{\mathfrak{B}}_{\varsigma\mathscr{G}}(\omega) \right\rangle.$$

Meanwhile,

$$\begin{aligned}(\overline{\mathfrak{T}}(\mathscr{G}))^c(\varphi) &= \left\langle \overline{\mathfrak{B}}_{\varkappa\mathscr{G}}(\varphi), \overline{\mathfrak{B}}_{\varrho\mathscr{G}}(\varphi), \overline{\mathfrak{B}}_{\varsigma\mathscr{G}}(\varphi) \right\rangle \\ &= \left\langle \bigwedge_{\omega\in[\varphi]_\simeq} \varkappa_\Upsilon(\omega), \bigwedge_{\omega\in[\varphi]_\simeq} \varrho_\Upsilon(\omega), \bigvee_{\omega\in[\varphi]_\simeq} \varsigma_\Upsilon(\omega) \right\rangle.\end{aligned}$$

Both expressions coincide, so

$$\underline{\mathfrak{T}}(\mathscr{G}^c) = (\overline{\mathfrak{T}}(\mathscr{G}))^c.$$

(3) A parallel argument gives

$$\begin{aligned}\overline{\mathfrak{T}}(\mathscr{G}^c)(\varphi) &= \left\langle \bigvee_{\omega\in[\varphi]_\simeq} \underline{\mathfrak{B}}_{\varkappa\mathscr{G}}(\omega), \bigvee_{\omega\in[\varphi]_\simeq} \underline{\mathfrak{B}}_{\varrho\mathscr{G}}(\omega), \bigwedge_{\omega\in[\varphi]_\simeq} \underline{\mathfrak{B}}_{\varsigma\mathscr{G}}(\omega) \right\rangle \\ &= \left\langle \overline{\mathfrak{B}}_{\varkappa\mathscr{G}}(\varphi), \overline{\mathfrak{B}}_{\varrho\mathscr{G}}(\varphi), \overline{\mathfrak{B}}_{\varsigma\mathscr{G}}(\varphi) \right\rangle^c = (\underline{\mathfrak{T}}(\mathscr{G}))^c(\varphi).\end{aligned}$$

(4) Let

$$x = \langle \varsigma_x, \varrho_x, \varkappa_x \rangle$$

be any q-ROSFS value on a vertex or an edge. Since

$$x^c = \langle \varkappa_x, \varrho_x, \varsigma_x \rangle,$$

Definition 14 gives

$$\begin{aligned}\mathcal{S}(x^c) &= \frac{1 + (\varkappa_x)^q - (\varsigma_x)^q}{2} \\ &= 1 - \frac{1 + (\varsigma_x)^q - (\varkappa_x)^q}{2} \\ &= 1 - \mathcal{S}(x).\end{aligned}$$

Thus the statement holds for both the vertex and edge values because the complement swaps the positive and negative components while keeping the neutral component unchanged.

This completes the proof. □

4. Application of the q-ROSFRG to agricultural irrigation network selection

The application problem is to select the most reliable connected irrigation route from a water source zone to a target farmland zone. The decision is not a conventional alternative ranking problem: Each feasible solution must be a continuous path in the network, and a single weak channel can reduce the reliability of the entire route. Uncertainty arises from expert judgments about the water availability, maintenance cost, water quality, climate compatibility, environmental impact, and social acceptability. Additional granularity arises because zones with similar soil characteristics may be indistinguishable for irrigation planning and are therefore represented as equivalence classes in the rough approximation space.

The q-ROSFRG model addresses this setting by combining q-rung orthopair spherical fuzzy information with rough approximations over a graph. Positive, neutral, and negative memberships describe the quality of vertices and channels; lower and upper approximations distinguish guaranteed from possible network information; and the maximin path-strength criterion selects a route whose weakest channel is as strong as possible. The following case study considers 10 agricultural zones connected by 20 irrigation channels and partitioned into 8 soil-based equivalence classes. The calculations are presented step by step to support reproducibility and to show how the proposed model preserves the network topology during decision-making.

4.1. The q-ROSFRG-based MCGDM algorithm

The q-ROSFRG-based MCGDM algorithm is, to a large extent, a natural offshoot of both the q-ROSFRG framework and the construction of MCGDM, because it integrates the q-ROSFRG framework into the process of choosing the irrigation path in a neat way. The method can be divided into six stages, which are described below and illustrated in Figure 5.

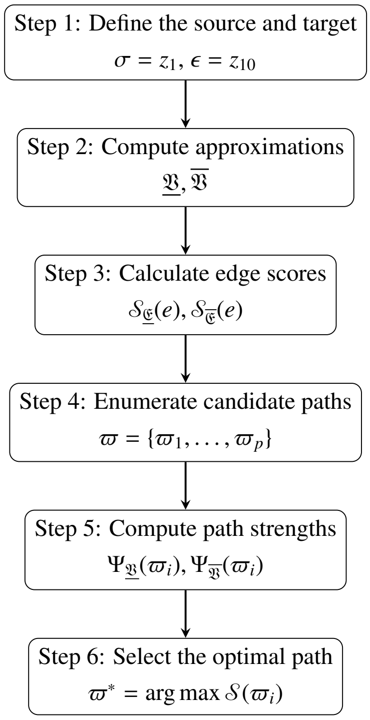

Figure 5. Flowchart of the q-ROSFRG-based MCGDM algorithm.

- Let $\aleph = \{z_1, z_2, \ldots, z_{10}\}$ be the set of agricultural zones.
- Let $\ell \subseteq \aleph \times \aleph$ be the set of irrigation channels.
- Let $\simeq$ be an equivalence relation on $\aleph$ (soil type classes, Table 4).
- Let $\Upsilon(z) = \langle \varsigma_\Upsilon(z), \varrho_\Upsilon(z), \varkappa_\Upsilon(z) \rangle$ be the q-ROSFS value of each zone (Table 5).

- Let $\Delta(uv) = \langle \varsigma_\Delta(uv), \varrho_\Delta(uv), \varkappa_\Delta(uv) \rangle$ be the q-ROSFS value of each channel, aggregated using the weights $W = (0.30, 0.20, 0.15, 0.20, 0.15)$ (Table 6).
- Let $\sigma = z_1$ and $\epsilon = z_{10}$ denote the source and target zones.
- Let $q = 2$ be the fixed parameter.

The proposed MCGDM process is summarized in Algorithm 1 below.

Algorithm 1: q-ROSFRG-based MCGDM algorithm.

Input:
- Network $\mathscr{G}^* = (\aleph, \ell)$, $|\aleph| = n$, $|\ell| = m$
- Equivalence relation $\simeq$ on $\aleph$ (soil type classes)
- Vertex memberships $\Upsilon(v) = \langle \varsigma_\Upsilon(v), \varrho_\Upsilon(v), \varkappa_\Upsilon(v) \rangle$
- Edge memberships $\Delta(uv) = \langle \varsigma_\Delta(uv), \varrho_\Delta(uv), \varkappa_\Delta(uv) \rangle$
- Source zone σ and target zone ϵ
- Parameter $q \geq 1$

Output: Optimal path ϖ^*

Step 1 (Define source and target): Identify the source zone $\sigma = z_1$ and the target zone $\epsilon = z_{10}$.

Step 2 (Compute approximations): For each vertex $\varphi \in \aleph$ and each edge $\omega\wp \in \ell$, compute the lower and upper approximations using Definition 10.

Step 3 (Calculate edge scores): For each edge $\omega\wp \in \ell$, compute the score function (Definition 14).

Step 4 (Enumerate candidate paths): Identify all simple paths $\varpi = \{\varpi_1, \ldots, \varpi_p\}$ from σ to ϵ.

Step 5 (Compute path strengths): For each candidate path ϖ_i, compute

$$\Psi_{\underline{\mathfrak{B}}}(\varpi_i) = \bigwedge_{e \in \varpi_i} \mathcal{S}_{\underline{\mathfrak{E}}}(e), \qquad \Psi_{\overline{\mathfrak{B}}}(\varpi_i) = \bigwedge_{e \in \varpi_i} \mathcal{S}_{\overline{\mathfrak{E}}}(e).$$

Step 6 (Select optimal path): Select the path with the highest score

$$\varpi^* = \arg\max_i \frac{\Psi_{\underline{\mathfrak{B}}}(\varpi_i) + \Psi_{\overline{\mathfrak{B}}}(\varpi_i)}{2}.$$

4.2. Detailed explanation of algorithmic steps

The MCGDM algorithm is developed to integrate the q-ROSFRG framework at decision level in a systematic way. The procedure can be divided into the following six main steps.

Step 1. Define the source and target: The choice is determined by considering the source zone of the irrigation water and the target zone where the water must flow to. Here, the water source is zone z_1, i.e., the reservoir's location. The purpose is zone z_{10}, which is the main farmland area to be irrigated. This step is crucial, as all other computations depend on these two points of reference.

Step 2. Compute the lower and upper approximations: In this step, the lower and upper approximations for all vertices, which represent agricultural zones, and all edges, representing irrigation channels, are calculated. The lower approximation expresses what is definite in terms of the membership information by applying the minimum operator to the positive and neutral memberships and the maximum operator to the negative membership in each equivalence class. In a similar way, the upper approximation represents what could be in terms of the membership information by applying the maximum operator to the positive and neutral memberships and the minimum operator to the negative membership. These approximations deal with uncertainties because of the similar soil types in different zones.

Step 3. Calculate the edge scores: After computing the lower and upper approximations for each edge, we map each three-dimensional q-ROSFS value to a single scalar score by using the score function. This rating indicates the reliability or quality of an irrigation channel as a whole. A higher score indicates better performance; a lower score indicates worse performance. This allows for a future comparison of different channels.

Step 4. Enumerate the candidate paths: In this step, we enumerate all the simple paths from a source zone z_1 to a destination zone z_{10}. A simple path is a sequence of vertices, any two consecutive vertices of which are joined by an edge, and where all vertices are distinct. The network's topology determines which routes can be used. In this application, we have five candidate paths, each representing a distinct pathway for delivering water from source to sink.

Step 5. Calculation of path strength: In the maximin method, the strength of a path is the smallest edge strength on the path. Such a precautionary approach is particularly suitable for farm irrigation systems, since a single channel break could risk the entire route. For each possible path, we have to compute two strengths, one using the lower approximation values and the other using the upper approximation values. This enables us to provide a pessimistic and optimistic view of path reliability.

Step 6. Select the optimal path: The final score of each path is then calculated as the average of the lower and upper strengths; the pessimistic and optimistic opinions are balanced. The maximum between the two values corresponds to the score of the best path, which determines the best irrigation path. If ties occur, additional arguments such as path length or the accuracy function can be used to choose among the best.

4.3. Illustrative example

This subsection provides a comprehensive, step-by-step demonstration of the proposed q-ROSFRG-based MCGDM framework through a case study selecting the optimal irrigation path in an agricultural network with ten zones. Consider a farmland consisting of 10 watering zones,

$$\aleph = \{z_1, z_2, z_3, z_4, z_5, z_6, z_7, z_8, z_9, z_{10}\},$$

connected by water channels

$$\ell \subseteq \aleph \times \aleph$$

as shown in Figure 6. The regions are divided into equivalence classes by soil types through the relation $\simeq$.

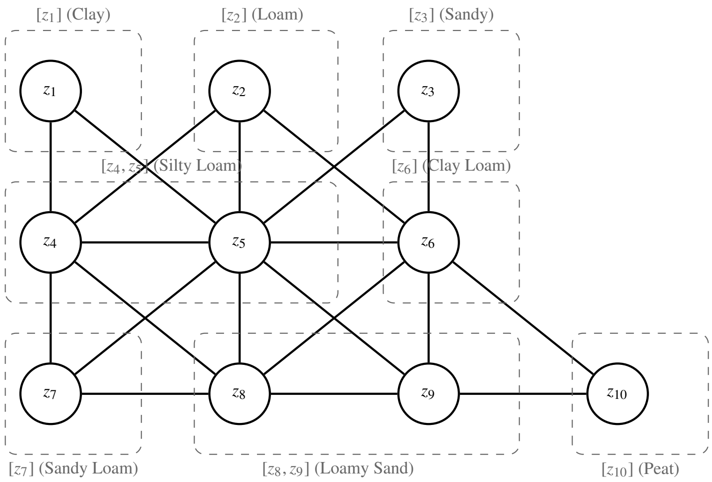

Figure 6. Irrigation network with 10 zones and $\simeq$-based equivalence classes

The equivalence relation $\simeq$ partitions the vertex set $\aleph$ according to soil type, as shown in Table 4.

Table 4. Equivalence classes based on soil type.

Zone	Soil type	Equivalence class $[z]_{\simeq}$
z_1	Clay soil	$\{z_1\}$
z_2	Loam soil	$\{z_2\}$
z_3	Sandy soil	$\{z_3\}$
z_4, z_5	Silty loam soil	$\{z_4, z_5\}$
z_6	Clay loam soil	$\{z_6\}$
z_7	Sandy loam soil	$\{z_7\}$
z_8, z_9	Loamy sand soil	$\{z_8, z_9\}$
z_{10}	Peat soil	$\{z_{10}\}$

Table 5 presents the q-ROSFS values for each agricultural zone, representing crop health indices based on historical data and expert assessments with $q = 2$.

Table 5. Vertex membership values Υ for each agricultural zone ($q = 2$).

Zone	$\varsigma_{\Upsilon}(z)$	$\varrho_{\Upsilon}(z)$	$\varkappa_{\Upsilon}(z)$
z_1	0.85	0.10	0.15
z_2	0.78	0.12	0.10
z_3	0.60	0.20	0.30
z_4	0.72	0.14	0.14
z_5	0.68	0.16	0.16
z_6	0.75	0.13	0.12
z_7	0.65	0.18	0.17
z_8	0.70	0.15	0.15
z_9	0.62	0.19	0.19
z_{10}	0.80	0.11	0.09

Table 6 presents the q-ROSFS values for each irrigation channel, aggregated from expert evaluations across five criteria.

Table 6. Edge membership values Δ for each irrigation channel (q = 2).

Edge	ς	ϱ	$\varkappa$
e_{14}	0.7200	0.1650	0.2350
e_{15}	0.6900	0.1700	0.2500
e_{24}	0.7000	0.1600	0.2400
e_{25}	0.6800	0.1750	0.2600
e_{26}	0.6500	0.1800	0.2700
e_{35}	0.6200	0.1900	0.2900
e_{36}	0.6000	0.1950	0.3100
e_{45}	0.7100	0.1550	0.2300
e_{47}	0.6700	0.1850	0.2800
e_{48}	0.6600	0.1880	0.2850
e_{57}	0.6400	0.1920	0.2950
e_{58}	0.6300	0.1940	0.3000
e_{59}	0.6100	0.1960	0.3150
e_{68}	0.5900	0.2000	0.3200
e_{69}	0.5800	0.2020	0.3250
$e_{6,10}$	0.5700	0.2050	0.3300
e_{56}	0.6400	0.1900	0.2900
e_{78}	0.6600	0.1850	0.2800
e_{89}	0.6400	0.1900	0.2900
$e_{9,10}$	0.6300	0.1920	0.2950

For instance, edges with lower membership values (e.g., $e_{6,10}$) represent less reliable irrigation channels due to higher cost, lower water quality, or environmental constraints.

Step 1: define source and target zones.

The irrigation water flows from zone z_1 (water source) to zone z_{10} (the main farm area). Thus, we set

$$\sigma = z_1, \quad \epsilon = z_{10}.$$

Step 2: compute upper and lower approximations.

Following Definition 10, we compute the lower and upper approximations for the vertices and edges using Eqs (3.1) and (3.2).

The lower vertex approximations are presented in Table 7.

Table 7. Lower vertex approximations $\underline{\mathfrak{V}}$.

Zone	$\underline{\mathfrak{V}}_{\varsigma}$	$\underline{\mathfrak{V}}_{\varrho}$	$\underline{\mathfrak{V}}_{\varkappa}$
z_1	0.85	0.10	0.15
z_2	0.78	0.12	0.10
z_3	0.60	0.20	0.30
z_4	0.68	0.14	0.16
z_5	0.68	0.14	0.16
z_6	0.75	0.13	0.12
z_7	0.65	0.18	0.17
z_8	0.62	0.15	0.19
z_9	0.62	0.15	0.19
z_{10}	0.80	0.11	0.09

The upper vertex approximations are presented in Table 8.

Table 8. Upper vertex approximations $\overline{\mathfrak{V}}$.

Zone	$\overline{\mathfrak{V}}_{\varsigma}$	$\overline{\mathfrak{V}}_{\varrho}$	$\overline{\mathfrak{V}}_{\varkappa}$
z_1	0.85	0.10	0.15
z_2	0.78	0.12	0.10
z_3	0.60	0.20	0.30
z_4	0.72	0.16	0.14
z_5	0.72	0.16	0.14
z_6	0.75	0.13	0.12
z_7	0.65	0.18	0.17
z_8	0.70	0.19	0.15
z_9	0.70	0.19	0.15
z_{10}	0.80	0.11	0.09

The lower edge approximations are presented in Table 9.

Table 9. Lower edge approximations $\underline{\mathfrak{E}}$.

Edge	$\underline{\mathfrak{E}}_{\varsigma}$	$\underline{\mathfrak{E}}_{\varrho}$	$\underline{\mathfrak{E}}_{\varkappa}$
e_{14}	0.6900	0.1650	0.2500
e_{15}	0.6900	0.1650	0.2500
e_{24}	0.6800	0.1600	0.2600
e_{25}	0.6800	0.1600	0.2600
e_{26}	0.6500	0.1800	0.2700
e_{35}	0.6200	0.1900	0.2900
e_{36}	0.6000	0.1950	0.3100
e_{45}	0.7100	0.1550	0.2300
e_{47}	0.6400	0.1850	0.2950
e_{48}	0.6100	0.1880	0.3150
e_{57}	0.6400	0.1850	0.2950
e_{58}	0.6100	0.1880	0.3150
e_{59}	0.6100	0.1880	0.3150
e_{68}	0.5800	0.2000	0.3250
e_{69}	0.5800	0.2000	0.3250
$e_{6,10}$	0.5700	0.2050	0.3300
e_{56}	0.6400	0.1900	0.2900
e_{78}	0.6600	0.1850	0.2800
e_{89}	0.6400	0.1900	0.2900
$e_{9,10}$	0.6300	0.1920	0.2950

The upper edge approximations are presented in Table 10.

Table 10. Upper edge approximations $\overline{\mathfrak{E}}$.

Edge	$\overline{\mathfrak{E}}_{\varsigma}$	$\overline{\mathfrak{E}}_{\varrho}$	$\overline{\mathfrak{E}}_{\varkappa}$
e_{14}	0.7200	0.1700	0.2350
e_{15}	0.7200	0.1700	0.2350
e_{24}	0.7000	0.1750	0.2400
e_{25}	0.7000	0.1750	0.2400
e_{26}	0.6500	0.1800	0.2700
e_{35}	0.6200	0.1900	0.2900
e_{36}	0.6000	0.1950	0.3100
e_{45}	0.7100	0.1550	0.2300
e_{47}	0.6700	0.1920	0.2800
e_{48}	0.6600	0.1960	0.2850
e_{57}	0.6700	0.1920	0.2800
e_{58}	0.6600	0.1960	0.2850
e_{59}	0.6600	0.1960	0.2850
e_{68}	0.5900	0.2020	0.3200
e_{69}	0.5900	0.2020	0.3200
$e_{6,10}$	0.5700	0.2050	0.3300
e_{56}	0.6400	0.1900	0.2900
e_{78}	0.6600	0.1850	0.2800
e_{89}	0.6400	0.1900	0.2900
$e_{9,10}$	0.6300	0.1920	0.2950

Step 3: calculate the edge scores.

Using the score function from Definition 14 with $q = 2$, we have the following

$$\mathcal{S}_{\underline{\mathfrak{E}}}(uv) = \frac{1 + (\underline{\mathfrak{E}}_{\varsigma}(uv))^2 - (\underline{\mathfrak{E}}_{\varkappa}(uv))^2}{2}, \quad \mathcal{S}_{\overline{\mathfrak{E}}}(uv) = \frac{1 + (\overline{\mathfrak{E}}_{\varsigma}(uv))^2 - (\overline{\mathfrak{E}}_{\varkappa}(uv))^2}{2}.$$

The calculated edge scores are presented in Table 11.

Table 11. Edge scores for lower and upper approximations ($q = 2$).

Edge	$\mathcal{S}_{\underline{\mathfrak{E}}}$	$\mathcal{S}_{\overline{\mathfrak{E}}}$
e_{14}	0.7068	0.7316
e_{15}	0.7068	0.7316
e_{24}	0.6974	0.7162
e_{25}	0.6974	0.7162
e_{26}	0.6748	0.6748
e_{35}	0.6502	0.6502
e_{36}	0.6320	0.6320
e_{45}	0.7256	0.7256
e_{47}	0.6613	0.6853
e_{48}	0.6364	0.6772
e_{57}	0.6613	0.6853
e_{58}	0.6364	0.6772
e_{59}	0.6364	0.6772
e_{68}	0.6154	0.6229
e_{69}	0.6154	0.6229
$e_{6,10}$	0.6080	0.6080
e_{56}	0.6628	0.6628
e_{78}	0.6786	0.6786
e_{89}	0.6628	0.6628
$e_{9,10}$	0.6549	0.6549

Step 4: enumerate the candidate paths.

The candidate paths from the source z_1 to destination z_{10} are listed in Table 12. The infeasible routes previously involving a non existing e_{12} connection have been removed; each route below starts at z_1, and each consecutive vertex pair is connected by an edge in Figure 6.

Table 12. Candidate paths from the source σ to destination ϵ.

Path	Sequence	Edges
ϖ_1	$z_1 \to z_4 \to z_5 \to z_8 \to z_9 \to z_{10}$	$\{e_{14}, e_{45}, e_{58}, e_{89}, e_{9,10}\}$
ϖ_2	$z_1 \to z_4 \to z_7 \to z_8 \to z_9 \to z_{10}$	$\{e_{14}, e_{47}, e_{78}, e_{89}, e_{9,10}\}$
ϖ_3	$z_1 \to z_5 \to z_6 \to z_{10}$	$\{e_{15}, e_{56}, e_{6,10}\}$
ϖ_4	$z_1 \to z_5 \to z_8 \to z_9 \to z_{10}$	$\{e_{15}, e_{58}, e_{89}, e_{9,10}\}$
ϖ_5	$z_1 \to z_4 \to z_8 \to z_9 \to z_{10}$	$\{e_{14}, e_{48}, e_{89}, e_{9,10}\}$

Step 5: compute the path strengths.

Following Definition 17, the strength of a path is defined as the minimum edge score along that path

$$\Psi_{\underline{\mathfrak{B}}}(\varpi_i) = \bigwedge_{e\in\varpi_i} \mathcal{S}_{\underline{\mathfrak{E}}}(e), \qquad \Psi_{\overline{\mathfrak{B}}}(\varpi_i) = \bigwedge_{e\in\varpi_i} \mathcal{S}_{\overline{\mathfrak{E}}}(e).$$

The calculated path strengths are presented in Table 13.

Table 13. Path strengths for lower and upper approximations.

Path	Edges	$\Psi_{\underline{\mathfrak{B}}}(\varpi_i)$	$\Psi_{\overline{\mathfrak{B}}}(\varpi_i)$
ϖ_1	$e_{14}, e_{45}, e_{58}, e_{89}, e_{9,10}$	$\min(0.7068, 0.7256, 0.6364, 0.6628, 0.6549) = 0.6364$	$\min(0.7316, 0.7256, 0.6772, 0.6628, 0.6549) = 0.6549$
ϖ_2	$e_{14}, e_{47}, e_{78}, e_{89}, e_{9,10}$	$\min(0.7068, 0.6613, 0.6786, 0.6628, 0.6549) = 0.6549$	$\min(0.7316, 0.6853, 0.6786, 0.6628, 0.6549) = 0.6549$
ϖ_3	$e_{15}, e_{56}, e_{6,10}$	$\min(0.7068, 0.6628, 0.6080) = 0.6080$	$\min(0.7316, 0.6628, 0.6080) = 0.6080$
ϖ_4	$e_{15}, e_{58}, e_{89}, e_{9,10}$	$\min(0.7068, 0.6364, 0.6628, 0.6549) = 0.6364$	$\min(0.7316, 0.6772, 0.6628, 0.6549) = 0.6549$
ϖ_5	$e_{14}, e_{48}, e_{89}, e_{9,10}$	$\min(0.7068, 0.6364, 0.6628, 0.6549) = 0.6364$	$\min(0.7316, 0.6772, 0.6628, 0.6549) = 0.6549$

Step 6: select optimal path.

The final score for each path is the average of lower and upper strengths

$$\mathcal{S}(\varpi_i) = \frac{\Psi_{\underline{\mathfrak{B}}}(\varpi_i) + \Psi_{\overline{\mathfrak{B}}}(\varpi_i)}{2}.$$

Table 14 presents the final scores and ranking of all candidate paths.

Table 14. Final scores and ranking of candidate paths.

Rank	Path	$\Psi_{\underline{\mathfrak{B}}}$	$\Psi_{\overline{\mathfrak{B}}}$	$\mathcal{S}(\varpi_i)$
1	ϖ_2	0.6549	0.6549	0.6549
2	ϖ_1	0.6364	0.6549	0.6457
2	ϖ_4	0.6364	0.6549	0.6457
2	ϖ_5	0.6364	0.6549	0.6457
5	ϖ_3	0.6080	0.6080	0.6080

The optimal irrigation path is

$$\varpi_2 = z_1 \to z_4 \to z_7 \to z_8 \to z_9 \to z_{10}$$

with a final score of 0.6549. Figure 7 presents a normalized comparison of the path scores.

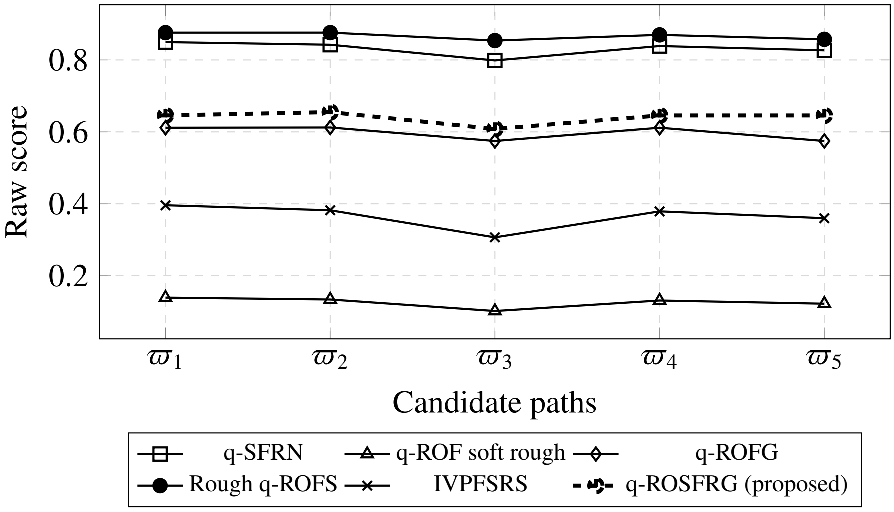

Figure 7. Comparison of scores across candidate paths for all models.

The selected path represents the strongest risk-averse route because its weakest channel score is higher than the weakest channel score of all other feasible paths. This confirms that the q-ROSFRG model can preserve connectivity while avoiding routes dominated by weak edges, such as those containing $e_{6,10}$.

The application results show that Algorithm 1 selects $\varpi_2 = z_1 \to z_4 \to z_7 \to z_8 \to z_9 \to z_{10}$ with a score of 0.6549. The corrected ranking places ϖ_1, ϖ_4, and ϖ_5 jointly after the optimal path with scores of 0.6457. The weakest candidate is ϖ_3, whose strength is limited by $e_{6,10}$. The example confirms that q-ROSFRG can rank feasible irrigation paths while respecting adjacency, equivalence classes, and soil type information in the network.

5. Comparative analysis and discussion

In this section, we validate the effectiveness and demonstrate the superiority of the proposed q-ROSFRG framework through a comprehensive comparative analysis. The comparison is divided into two main parts: (i) A theoretical feature-based comparison highlighting the structural and algebraic capabilities of each model, and (ii) a quantitative performance evaluation on the agricultural irrigation network dataset. The primary objective is to emphasize the unique characteristics of the q-ROSFRG framework, particularly its ability to solve network-based path optimization problems while preserving the topological connectivity constraints.

5.1. Overview of comparative methods

We compare the proposed q-ROSFRG model with a set of 10 existing approaches that reflect the evolution of uncertainty modeling, ranging from classical fuzzy representations to advanced hybrid frameworks. The comparison begins with foundational models such as FSs [1], which consider only membership degree, followed by IFSs [2], incorporating both membership and nonmembership under the constraint $\xi + \zeta \leq 1$. This is further extended by PFSs, which introduce a neutral degree with $\xi + \varrho + \zeta \leq 1$, and SFSs [7], which generalize the constraint to $\xi^2 + \varrho^2 + \zeta^2 \leq 1$. The q-ROFSs [10] enhance flexibility through the generalized constraint $\xi^q + \zeta^q \leq 1$.

In addition, several hybrid rough and soft set-based models are considered, including IVPFSRS [13], q-rung orthopair fuzzy soft rough sets [24], and rough q-ROFS [18], all of which are primarily designed for alternative selection problems under uncertainty. Furthermore, graph-based extensions are included in the comparison, such as q-rung orthopair fuzzy graphs (q-ROFGs) [22], which do not incorporate rough approximations, and SFRGs [8], representing a special case with a fixed $q = 2$.

Finally, the proposed q-ROSFRG model is introduced as a comprehensive framework that integrates flexible q-rung orthopair spherical fuzzy information with rough approximations and graph structures, while incorporating two-stage approximation mechanisms and a maximin path strength criterion, thereby enabling effective modeling of optimal path selection problems under uncertainty.

5.2. *Feature-based comparative analysis*

Table 15 displays a detailed comparison of all 11 models on a feature-by-feature basis. The comparison focuses on four main features: (1) Representation of uncertainty, (2) theoretical base, (3) graph and network operations, and (4) class of problem.

Table 15. Comparative analysis of q-ROSFRG and existing models.

Feature	FS	IFS	PFS	SFS	q-ROFS	IVPFSRS	q-ROF soft rough	Rough q-ROFS	q-ROFG	SFRG	q-ROSFRG (proposed)
						Uncertainty representation					
Membership (ξ)	✓	✓	✓	✓	✓	✓	✓	✓	✓	✓	✓
Nonmembership (ζ)	✗	✓	✓	✓	✓	✓	✓	✓	✓	✓	✓
Neutral/hesitation (ϱ)	✗	✗	✓	✓	✗	✓	✗	✗	✗	✓	✓
Interval-valued support	✗	✗	✗	✗	✗	✓	✗	✗	✗	✗	✗
q-Rung constraint	✗	✗	✗	✗	✓	✗	✓	✓	✓	✗	✓
						Theoretical framework					
Rough set approximations	✗	✗	✗	✗	✗	✓	✓	✓	✗	✓	✓
Soft set parameterization	✗	✗	✗	✗	✗	✓	✓	✗	✗	✗	✗
Equivalence relations for granularity	✗	✗	✗	✗	✗	✓	✓	✓	✗	✓	✓
						Graph and network capabilities					
Graph/network structure	✗	✗	✗	✗	✗	✗	✗	✗	✓	✓	✓
Vertex membership functions	✗	✗	✗	✗	✗	✗	✗	✗	✓	✓	✓
Edge membership functions	✗	✗	✗	✗	✗	✗	✗	✗	✓	✓	✓
Source-target path enumeration	✗	✗	✗	✗	✗	✗	✗	✗	✓	✓	✓
Connectivity constraint preservation	✗	✗	✗	✗	✗	✗	✗	✗	✓	✓	✓
Two-stage approximations (vertices then edges)	✗	✗	✗	✗	✗	✗	✗	✗	✗	✗	✓
Maximin path strength criterion	✗	✗	✗	✗	✗	✗	✗	✗	✗	✗	✓
						Problem and application					
Problem type						Alternative selection			Path selection		
Data structure						Decision matrix			Graph $(\aleph, \ell)$		
Output						Best alternative			Best path ($\sigma \to \epsilon$)		
Application						Supplier/personnel			Irrigation network		

As shown in Table 15, the proposed q-ROSFRG framework exhibits several distinctive characteristics that set it apart from all existing models.

(1) Complete graph topology: Unlike alternative selection models, the q-ROSFRG incorporates vertex and edge membership functions, preserving the network structure and connectivity

constraints.

(2) Flexible q-rung three-dimensional representation: While the SFRG model uses a fixed spherical constraint ($q = 2$) and the q-ROFG model lacks neutral membership, the q-ROSFRG model simultaneously provides three-dimensional membership (ξ, ϱ, ζ) and a flexible q-rung constraint adjustable to different levels of uncertainty.

(3) Two-stage rough approximations: Unlike the q-ROFG and SFRG models, the q-ROSFRG performs rough approximations at both the vertex level (based on equivalence classes such as soil type) and the edge level, capturing granularity in the network data.

(4) Maximin path optimization: This is the first framework to introduce a maximin path strength criterion specifically for risk-averse infrastructure planning, ensuring that the weakest edge determines the overall path reliability.

5.3. Quantitative comparison and analysis

To quantitatively evaluate the proposed framework, we compare it against several state-of-the-art models using an agricultural irrigation network dataset consisting of 10 vertices, 20 edges, and 5 candidate paths. The comparative models include the q-spherical fuzzy rough Einstein (q-SFRN) model [23], q-rung orthopair fuzzy soft rough sets [24], q-rung orthopair fuzzy graphs (q-ROFGs) [22], rough q-ROFSs [18], and IVPFSRSs [13], in addition to the proposed q-ROSFRG model. For models originally designed for alternative selection, including the q-SFRN, q-ROF soft rough set, and IVPFSRS models, each candidate path was treated as an independent alternative using average aggregation. In contrast, for graph-based models such as the q-ROFG, rough q-ROFS, and the proposed q-ROSFRG models, the underlying network topology was preserved and the maximin criterion was applied to evaluate paths' reliability. Table 16 reports the raw path scores obtained from all six models across the five candidate paths. These scores are computed directly from the respective algorithms without normalization in order to preserve the original scale and enable a fair and direct comparison.

Table 16. Quantitative results an irrigation network.

Model	ϖ_1	ϖ_2	ϖ_3	ϖ_4	ϖ_5	Best
q-SFRN [23]	**0.84959**	0.84229	0.79859	0.83868	0.82671	ϖ_1
q-ROF Soft Rough [24]	**0.13912**	0.13390	0.10190	0.13112	0.12223	ϖ_1
q-ROFG [22]	0.61152	**0.61219**	0.57463	0.61152	0.57463	ϖ_2
Rough q-ROFS [18]	0.87590	**0.87595**	0.85386	0.86970	0.85733	ϖ_2
IVPFSRS [13]	**0.39600**	0.38200	0.30667	0.37900	0.36000	ϖ_1
q-ROSFRG (proposed)	0.64569	**0.65494**	0.60800	0.64569	0.64569	ϖ_2

It is worth noting that the proposed q-ROSFRG model produces scores based on the maximin criterion with flexible q-rung spherical fuzzy information. The results reveal that three out of six models (q-ROFG, rough q-ROFS, and the proposed q-ROSFRG) consistently identify ϖ_2 as the optimal path, while the remaining three models (q-SFRN, q-ROF soft rough sets, IVPFSRS) favor ϖ_1. This indicates a clear consensus among models that preserve the graph topology and use risk-averse aggregation strategies.

To better visualize the comparative behavior of the six evaluated models (q-SFRN, q-ROF soft rough, q-ROFG, rough q-ROFS, IVPFSRS, and the proposed q-ROSFRG) across the five candidate paths, a line plot representation is provided in Figure 7. This graphical illustration highlights the variation in the score distributions for each model and clearly shows the differences in their decision patterns under uncertainty. In particular, it facilitates the identification of the most preferred paths and reveals the consistency of graph-based models (q-ROFG and the proposed q-ROSFRG) compared with alternative selection approaches (q-SFRN, q-ROF soft rough, IVPFSRS).

As illustrated in Figure 7, there is a noticeable distinction in the behavior of different models over the candidate paths. Graph-based models (q-ROFG and the proposed q-ROSFRG) exhibit consistent performance trends and tend to agree on ϖ_2 as the optimal path, while aggregation-based models (q-SFRN, q-ROF soft rough, IVPFSRS) show greater variability and favor ϖ_1 instead. The rough q-ROFS model, which combines lower and upper approximations, achieves the highest raw scores but also identifies ϖ_2 as the best path. This confirms the influence of structural information in maintaining stable and reliable decision-making under uncertainty.

5.3.1. Analysis by aggregation strategy

The results reveal a clear distinction among models based on their aggregation strategy. Models using the maximin criterion (q-ROFG and the proposed q-ROSFRG) consistently identify ϖ_2 as the optimal path, as shown in Table 17. This consistent behavior indicates that, in risk-sensitive network environments, decision-making is primarily governed by the strength of the weakest link, where ensuring minimum reliability across all edges becomes the dominant factor in selecting the optimal route.

Table 17. Maximin-based model comparison.

Model	ϖ_1	ϖ_2	ϖ_3	ϖ_4	ϖ_5	Best
q-ROFG	0.61152	**0.61219**	0.57463	0.61152	0.57463	ϖ_2
q-ROSFRG (proposed)	0.64569	**0.65494**	0.60800	0.64569	0.64569	ϖ_2

This agreement confirms that ϖ_2 is the most reliable route under the worst-case (bottleneck) evaluation, which is essential in infrastructure applications. In contrast, models using average aggregation (q-SFRN, q-ROF Soft Rough Sets, and IVPFSRS) favor ϖ_1, as shown in Table 18, since these approaches prioritize overall accumulated performance across edges rather than focusing on the weakest link constraint, leading to different decision outcomes compared with maximin-based models.

Table 18. Comparison of average-based models.

Model	ϖ_1	ϖ_2	ϖ_3	ϖ_4	ϖ_5	Best
q-SFRN	**0.84959**	0.84229	0.79859	0.83868	0.82671	ϖ_1
q-ROF soft rough	**0.13912**	0.13390	0.10190	0.13112	0.12223	ϖ_1
IVPFSRS	**0.39600**	0.38200	0.30667	0.37900	0.36000	ϖ_1

The rough q-ROFS model, which incorporates the lower and upper approximations, also selects ϖ_2 (Table 19), further supporting the robustness of this result.

Table 19. Rough q-ROFS results.

Model	ϖ_1	ϖ_2	ϖ_3	ϖ_4	ϖ_5	**Best**
Rough q-ROFS	0.87590	**0.87595**	0.85386	0.86970	0.85733	ϖ_2

5.3.2. Why does ϖ_2 outperform ϖ_1?

An edge-level comparison (Table 20) shows that both paths share the same minimum strength (0.63), but ϖ_2 has a more balanced distribution of edge weights, leading to a slightly higher maximin score (0.65494 vs. 0.64569). This balance improves overall reliability under worst-case evaluation.

Table 20. Edge-level comparison of ϖ_1 and ϖ_2.

Path	Edge 1	Edge 2	Edge 3	Edge 4	Edge 5	Min
ϖ_1	e14 (0.71)	e45 (0.73)	e58 (0.64)	e89 (0.66)	e9_10 (0.65)	0.64
ϖ_2	e14 (0.71)	e47 (0.66)	e78 (0.68)	e89 (0.66)	e9_10 (0.65)	0.65

Overall, the analysis demonstrates that aggregation strategy is the key factor influencing the final decision: Maximin-based models prioritize reliability and consistently select ϖ_2, while average-based models favor overall strength and select ϖ_1. For infrastructure systems, the maximin strategy is more suitable as it accounts for the system's robustness in the presence of failures.

6. Limitations and future work

Although the proposed q-ROSFRG framework provides an effective approach for uncertainty-aware network path optimization, several limitations should be acknowledged. They are primarily related to the computational complexity, data requirements, parameter sensitivity, and theoretical assumptions.

6.1. Limitations

From a computational point of view, the main bottleneck is path enumeration, which grows exponentially with the size of the network. A brute-force search is not feasible even for networks of moderate size. The time complexity drastically increases when moving from small-scale to large-scale networks, as recapitulated in Table 21, and may be as large as $O(10^6)$ operations. This strongly suggests that scalability remains an issue for extremely large infrastructure systems when using the proposed framework.

Table 21. Complexity analysis across scales.

Scale category	Vertices (n)	Edges (m)	Time complexity
Small-scale	$n \leq 10$	$m \leq 20$	$O(10^2)$
Medium-scale	$n \leq 50$	$m \leq 100$	$O(10^4)$
Large-scale	$n > 100$	$m > 500$	$O(10^6)$

In addition, the computation of two-stage rough approximations and q-rung operations increases the processing cost compared with classical fuzzy graph models. The framework also requires rich and precise input data, including full membership degrees for the vertices and edges. As shown in Table 22, this leads to higher data acquisition effort compared with traditional fuzzy graph approaches, which may limit the model's applicability in environments with incomplete or noisy data.

Table 22. Data requirements across fuzzy graph frameworks.

Model	Components per assessment	Data effort
Fuzzy graphs (FG)	1	Very low
Intuitionistic fuzzy graphs (IFG)	2	Low
Spherical fuzzy graphs (SFG)	3	Medium
q-ROF graphs (q-ROFG)	2	Low
q-ROSFRG (proposed)	**6**	**High**

Moreover, the parameters q and η significantly influence the final results, while no systematic and universally accepted method currently exists for their optimal selection. The model also assumes that the network structure is fixed, that there is a single source–target pair, and that the edge memberships are independent. These assumptions may limit the model's use in unpredictable or strongly interconnected real systems. Finally, although the multidimensional feature of the model enables sufficient mathematical richness, it may affect interpretability for non expert users.

6.2. Future work

Future research will focus on improving scalability through heuristic and metaheuristic path search methods, as well as parallel and distributed computation techniques. These enhancements are vital to enable the model to be applied to large networks. Theoretical extensions cover tolerance-based approximations, the modeling of correlated edges, other aggregation operators, and K-best path forms. Parameter tuning is another major avenue, including automatic determination of q and η from a data-centric or learning-centric point of view. Lastly, Table 23 presents a summarization of the potential research trends and their implications, demonstrating how each direction leads to better scalability, interpretability, and practical applicability.

Table 23. Future research directions and impacts.

Direction	Methodological steps	Expected impact
Algorithmic improvements	Heuristic search, parallel computing, incremental updates	Scalability to large networks
Theoretical extensions	Dynamic networks, K-best paths, tolerance relations	Broader applicability
Parameter optimization	Automatic q and η selection	Reduced subjectivity
Interpretability	Visualization and explanation tools	Better usability
Application expansion	Energy, transport, healthcare, telecom networks	Real-world validation

Overall, addressing these limitations and exploring the proposed future directions will significantly enhance the robustness, efficiency, and practical impact of the q-ROSFRG framework in complex uncertain network environments.

7. Conclusions

This paper introduced the q-ROSFRG framework for source-to-target path optimization under uncertainty. Unlike traditional fuzzy rough decision-making models that rank independent alternatives, the proposed framework evaluates connected paths while preserving the topology of the underlying graph. This shift from alternative selection to topology-preserving path selection is the central contribution of the study.

The proposed model combines three complementary mechanisms. First, q-rung orthopair SFSs represent positive, neutral, and negative information under a tunable admissibility constraint. Second, rough lower and upper approximations capture the granularity generated by equivalence classes such as soil type classes. Third, the graph-theoretic structure keeps the vertices, edges, neighborhoods, and feasible paths explicit. On the basis of these components, we developed approximation operators, algebraic operations, score and accuracy functions, vertex degree, connectedness, similarity measures, complement properties, and a maximin path strength procedure.

The agricultural irrigation case study demonstrated the practical use of the model on a network with 10 zones and 20 irrigation channels. Using the corrected path enumeration in which ϖ_4 and ϖ_5 no longer use the non existing $z_1 \to z_2$ connection, the optimal route remained $\varpi_2 = z_1 \to z_4 \to z_7 \to z_8 \to z_9 \to z_{10}$, with a final score of 0.6549. The corrected calculations, based on the table values reproduced from the reference file and valid route adjacency, show that paths containing weaker edges, especially $e_{6,10}$, obtain lower scores under the maximin criterion.

The advantages of the q-ROSFRG model are its ability to model three-dimensional uncertainty, incorporate rough granularity, preserve network connectivity, and provide transparent route rankings. The main limitations are the computational cost of enumerating many paths in large networks, the dependence on expert-generated q-ROSFS values, sensitivity to the selected rung parameter q, and possible scalability issues when the equivalence classes are large. Future research may develop scalable shortest-path algorithms under q-ROSFRG information, dynamic versions for time-varying networks, adaptive methods for selecting q, and validation on larger irrigation, transportation, energy, and logistics networks.

Overall, the q-ROSFRG framework offers a unified and practically interpretable tool for uncertain network optimization problems in which preserving the connected structure of feasible solutions is essential.

Author contributions

Wedad Khaled Alshaman: conceptualization, methodology, investigation, and writing original draft; Kholood Alsager: supervision, conceptualization, writing review, and editing. All authors have read and agreed to the published version of the manuscript.

Use of Generative-AI tools declaration

The authors declare they have not used Artificial Intelligence (AI) tools in the creation of this article.

Funding

The researchers would like to thank the Deanship of Graduate Studies and Scientific Research at Qassim University (`www.qu.edu.sa`) for financial support (QU-APC-2026).

Conflict of interest

The authors declare no conflicts of interest.

References

1. L. A. Zadeh, Fuzzy sets, *Inf. Control*, **8** (1965), 338–353. https://doi.org/10.1016/S0019-9958(65)90241-X

2. K. T. Atanassov, *Intuitionistic fuzzy sets*, Springer, Physica-Verlag, 1999. https://doi.org/10.1007/978-3-7908-1870-3_1

3. Z. Pawlak, Rough sets, *Int. J. Comput. Inf. Sci.*, **11** (1982), 341–356. https://doi.org/10.1007/BF01001956

4. D. Dubois, H. Prade, Rough fuzzy sets and fuzzy rough sets, *Int. J. Gen. Syst.*, **17** (1990), 191–209. https://doi.org/10.1080/03081079008935107

5. M. I. Ali, F. Feng, X. Liu, W. K. Min, M. Shabir, On some new operations in soft set theory, *Comput. Math. Appl.*, **57** (2009), 1547–1553. https://doi.org/10.1016/j.camwa.2008.11.009

6. R. R. Yager, Pythagorean fuzzy subsets, *2013 Joint IFSA World Congress and NAFIPS Annual Meeting (IFSA/NAFIPS)*, 2013. https://doi.org/10.1109/IFSA-NAFIPS.2013.6608375

7. T. Mahmood, K. Ullah, Q. Khan, N. Jan, An approach toward decision-making and medical diagnosis problems using the concept of spherical fuzzy sets, *Neural Comput. Appl.*, **31** (2019), 7041–7053. https://doi.org/10.1007/s00521-018-3521-2

8. M. Akram, D. Saleem, T. Al-Hawary, Spherical fuzzy graphs with application to decision-making, *Math. Comput. Appl.*, **25** (2020), 8. https://doi.org/10.3390/mca25010008

9. R. R. Yager, Generalized orthopair fuzzy sets, *IEEE Trans. Fuzzy Syst.*, **25** (2017), 1222–1230. https://doi.org/10.1109/TFUZZ.2016.2604005

10. H. Garg, *q-rung orthopair fuzzy sets*, Springer, 2022. https://doi.org/10.1007/978-981-19-1449-2

11. T. Mahmood, J. Ahmmad, Z. Ali, D. Pamucar, D. Marinkovic, Interval valued T-spherical fuzzy soft average aggregation operators and their applications in multiple-criteria decision making, *Symmetry*, **13** (2021), 829. https://doi.org/10.3390/sym13050829

12. D. Molodtsov, Soft set theory–first results, *Comput. Math. Appl.*, **37** (1999), 19–31. https://doi.org//10.1016/S0898-1221(99)00056-5

13. R. M. Almozaini, K. M. Alsager, Interval-valued picture fuzzy soft rough sets: a new hybrid framework for robust multi-criteria group decision-making, *Symmetry*, **18** (2026), 419. https://doi.org/10.3390/sym18030419

14. S. Rizvi, H. J. Naqvi, D. Nadeem, Rough intuitionistic fuzzy sets, *Proceedings of the 6th Joint Conference on Information Sciences (JCIS)*, 2002, 101–104.

15. N. X. Thào, N. V. Đinh, Rough picture fuzzy set and picture fuzzy topologies, *J. Comput. Sci. Cybern.*, **31** (2015), 245. https://doi.org/10.15625/1813-9663/31/3/5046

16. S. A. Shanthi, M. Gayathri, Interval valued picture fuzzy soft set in pattern recognition, *Adv. Math.*, **9** (2020), 2019–2029. https://doi.org/10.37418/amsj.9.4.60

17. A. Tiwari, Q. D. Lohani, Interval-valued intuitionistic fuzzy rough set system over a novel conflict distance measure with application to decision-making, *MethodsX*, **10** (2023), 102012. https://doi.org/10.1016/j.mex.2023.102012

18. M. A. Bilal, M. Shabir, A. N. Al-Kenani, Rough q-rung orthopair fuzzy sets and their applications in decision-making, *Symmetry*, **13** (2021), 2010. https://doi.org/10.3390/sym13112010

19. A. Rosenfeld, Fuzzy graphs, *Fuzzy Sets Appl. Cognitive Dec. Process.*, 1975, 77–95. https://doi.org/10.1016/B978-0-12-775260-0.50008-6

20. H. Rashmanlou, S. Samanta, M. Pal, R. A. Borzooei, Intuitionistic fuzzy graphs with categorical properties, *Fuzzy Inf. Eng.*, **7** (2015), 317–334. https://doi.org/10.1016/j.fiae.2015.09.005

21. M. Akram, W. A. Dudek, Interval-valued fuzzy graphs, *Comput. Math. Appl.*, **61** (2011), 289–299. https://doi.org/10.1016/j.camwa.2010.11.004

22. M. Akram, M. Sitara, Decision-making with q-rung orthopair fuzzy graph structures, *Granul. Comput.*, **7** (2022), 505–526. https://doi.org/10.1007/s41066-021-00281-3

23. A. B. Azim, A. Ali, A. S. Khan, S. Ali, F. A. Awwad, E. A. A. Ismail, q-spherical fuzzy rough Einstein geometric aggregation operator for image understanding and interpretations, *IEEE Access*, **12** (2024), 140380–140411. https://doi.org/10.1109/ACCESS.2024.3423387

24. Y. Wang, A. Hussain, T. Mahmood, M. I. Ali, H. Wu, Y. Jin, Decision-making based on q-rung orthopair fuzzy soft rough sets, *Math. Probl. Eng.*, **2020** (2020), 6671001. https://doi.org/10.1155/2020/6671001

25. F. Karaaslan, F. Karamaz, Some new product operations of T-spherical fuzzy graphs and an application of T-spherical fuzzy graphs in MCGDM, *Artif. Intell. Rev.*, **56** (2023), 13663–13689. https://doi.org/10.1007/s10462-023-10477-5

26. Y. Rao, S. Kosari, S. Hameed, Z. Yousaf, Multi-attribute decision-making using q-rung orthopair fuzzy Zagreb index, *Artif. Intell. Rev.*, **58** (2025), 153. https://doi.org/10.1007/s10462-025-11149-2

27. D. Shi, S. E. Abbas, H. M. Khiamy, I. Ibedou, Fuzzy rough graphs via fuzzy graph ideals with applications, *AIMS Math.*, **11** (2026), 2979–3007. https://doi.org/10.3934/math.2026119

28. T. He, Rough properties of rough graph, *Appl. Mech. Mater.*, **157** (2012), 517–520. https://doi.org/10.4028/www.scientific.net/AMM.157-158.517